Science of the Total Environment 947 (2024) 174289

Contents lists available at ScienceDirect

Science of the Total Environment

journal homepage: www.elsevier.com/locate/scitotenv

Enhancing human resilience against climate change: Assessment of hydroclimatic extremes and sea level rise impacts on the Eastern Shore of Virginia, United States

Thanh-Nhan-Duc Tran [a,*], Venkataraman Lakshmi [a]

[a] Department of Civil and Environmental Engineering, University of Virginia, Charlottesville, VA 22904, USA

HIGHLIGHTS

- A transition between dry and wet conditions is found towards 2100
- Droughts are dominant in the 2020s to 2040s, whereas later periods are prone to severe floods
- Coastal regions are highly vulnerable to coastal- and sea level rise-induced flooding
- Need actions for climate resilience and adaptation to climate change

GRAPHICAL ABSTRACT

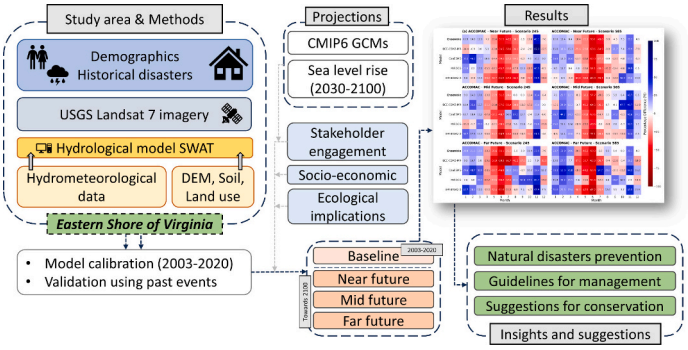

ARTICLE INFO

Editor: Christian Herrera

Keywords:
Climate change
Flood
Drought
Sea level rise
CMIP6
Resilience
Eastern Shore of Virginia

ABSTRACT

Coastal regions face climate-induced threats that have likely increased over the past four decades. In this work, we quantify the future climate impacts on hydroclimatic extremes in the risk-prone, 15-m-above-sea-level Eastern Shore of Virginia (ESVA) region, utilizing the Sixth International Coupled Model Intercomparison Project (CMIP6) Assessment Report 6 (AR6) and General Circulation Models (GCMs). We incorporate historical data on demographics and disasters, land use land cover (LULC), Landsat imagery, and sea level rise (SLR) to better understand and highlight the correlation between hydroclimatic extremes and societal components in this region. The hydrological model Soil and Water Assessment Tool (SWAT), Standardized Precipitation Index (SPI), Normalized Difference Water Index (NDWI), and Interquartile Range (IQR) method have been used to evaluate the intensity and frequency of projected climate extremes, in which SLR projections under different greenhouse gas emission pathways are temporally and spatially quantified. Our findings include (1) a trend towards wetter conditions is found with an increase in the number of flood events and up to an 8.9 % rise in the severity of flood peaks compared to the 2003–2020 period; (2) current coastal high-risk regions, identified using historical data of natural disasters, demographics, and LULC, are projected to be more susceptible to future climate impacts; and (3) low-lying coastal towns and regions are identified as currently vulnerable to coastal and SLR-induced flooding and are projected to become even more susceptible by 2100. This is the first effort that provides a valuable scientific basis for anticipated shifts in future climate patterns, essential for natural hazard prevention in

* Corresponding author.
E-mail address: syu3cs@virginia.edu (T.-N.-D. Tran).

https://doi.org/10.1016/j.scitotenv.2024.174289
Received 29 February 2024; Received in revised form 29 May 2024; Accepted 23 June 2024
Available online 27 June 2024

ESVA. It highlights the need for authorities and decision-makers to plan and implement adaptive strategies and sustainable policies for the ESVA region and other coastal areas across the United States.

1. Introduction

Climate change is projected to considerably impact the hydrological cycle, which is expected to further influence the redistribution of water resources. In 2023, the United States experienced 28 different weather and climate-related disasters with an estimated cost of at least one billion dollars (Smith, 2024). This marks the highest number of billion-dollar disasters ever recorded in a single year. Many previous studies have indicated that changes in the intensity and frequency of weather-related events could significantly impact both human society and the natural environment (Nguyen et al., 2023a; Bonsoms et al., 2023; Tran et al., 2021a, 2022c). To be specific, hydroclimatic extremes such as hurricanes, sea level rise (SLR), droughts, and floods, which vary spatially and temporally, can considerably impact local economies and communities (Nghia et al., 2022a; IPCC, 2023). For many regions, floods and droughts have been found to cause billions of dollars in damage (Ren et al., 2023; Tran et al., 2021b, 2023d; Nguyen et al., 2022a). These extremes are expected to be even more frequent and severe in coastal regions, primarily driven by increases in temperature and precipitation towards 2100 (IPCC, 2023; Saleem et al., 2021; Shrestha et al., 2018; Saeedi et al., 2023) as well as the combined impacts with future SLR (Rebecca, 2022).

The latest report by the Intergovernmental Panel on Climate Change (IPCC) on Ocean, Cryosphere, and Sea Level Change underscores the considerable rise in the severity of climate extremes due to the increases in meteorological variables (IPCC, 2023). The human-caused increase in greenhouse gases has been highlighted as intensifying the frequency and intensity of extreme weather events (IPPC, 2021), leading to more water-related issues (Rosenzweig and Neofotis, 2013; Nguyen et al., 2023b; Tran et al., 2022b). Specifically, the highest emission scenario predicts an increase of up to 5 °C (Hausfather, 2019; IPCC, 2021), in which we have only a 1 % chance of avoiding this phenomenon, with an average increase of at least 2.0 °C in the upcoming decades (Raftery et al., 2017). Notably, this rise is expected to significantly escalate the frequency and severity of floods, coastal flooding, and SLR in coastal regions (IPCC, 2021, 2023; Rebecca, 2022). In addition, low-lying coastal regions along America's East Coast have recently been found as facing more hidden vulnerabilities related to SLR (NASA, 2024; Ohenhen et al., 2023). It can be explained due to these regions' low elevation (Bailis et al., 2020; Toimil et al., 2020), the absence of natural barriers (O'Donoghue et al., 2021), and land degradation caused by extreme weather conditions (Webb et al., 2017).

Eastern Shore of Virginia (ESVA) is a low-lying coastal region, nestled between the Atlantic Ocean and Chesapeake Bay (Fig. 1). In recent years, this area has been increasingly threatened by climate change (Andrews et al., 2019; Sanford and Pope, 2010). Despite these threats, ESVA serves as a refuge for diverse habitats, including maritime forests, shrub thickets, grasslands, beaches, and tidal wetlands. These ecosystems are crucial for millions of migratory songbirds, raptors, shorebirds, and butterflies, providing essential resting and refueling points (U.S. Fish and Wildlife Service, 2018). Given its low elevation, ESVA is classified as high-risk and is currently vulnerable to climate

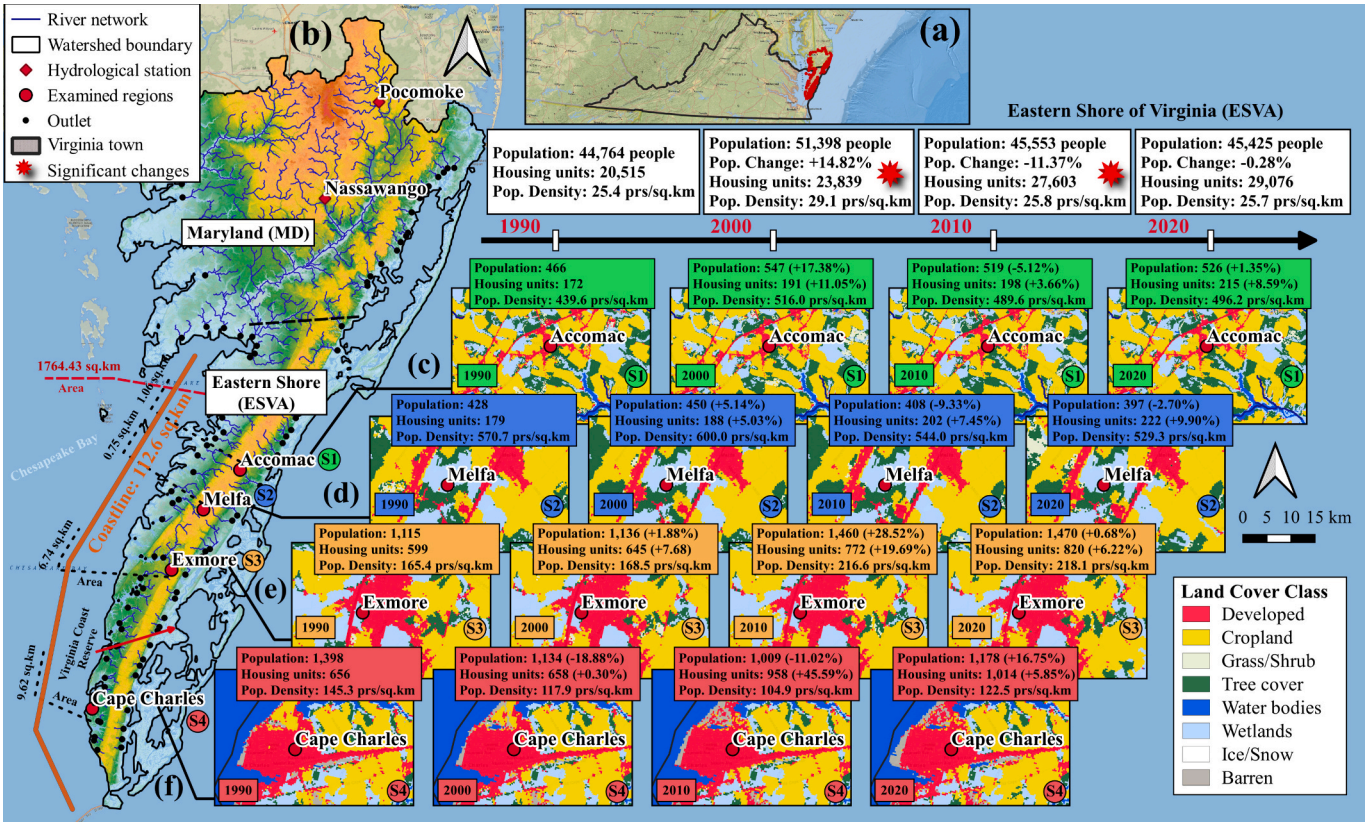

Fig. 1. (a) Location of MD-ESVA within the State of Virginia; (b) Terrain profile and geographical characteristics of MD-ESVA; (c-f) LULC changes and historical demographic changes (U.S Census Bureau, 2023), including (S1) Accomac, (S2) Melfa, (S3) Exmore, and (S4) Cape Charles, using the United States Geological Survey (USGS) Land Change Monitoring, Assessment, and Projection (LCMAP) datasets (1990–2020) (USGS, 2020). The percentage change (%) indicates the difference between two consecutive years.

change and SLR (Russ, 2020). These challenges are expected to be more severe under future climate scenarios (Russ, 2020; Sanford and Pope, 2007, 2010). Despite the critical need for scientific research in this region, the current literature is significantly limited, primarily conducted by regional agencies and departments (Chesapeake Bay Foundation, 2018; U.S. Fish and Wildlife Service, 2018), individuals (Nowroozi et al., 1999; Sanford and Pope, 2007, 2010), or academic institutions, e.g., University of Virginia (Russ, 2020; Zambello, 2019). Additionally, we found a noticeable absence of scientific efforts to quantify the projected impacts of future climate on current natural extremes. This thus underscores the urgent need to perform this work for the resilience of this ecologically diverse and economically significant region.

General Circulation Models, also known as Global Climate Models (GCMs), are commonly used to measure future projected impacts of hydroclimatic extremes (Neill et al., 2016; Tebaldi et al., 2021). The recent release of the Coupled Model Intercomparison Project Version 6 (CMIP6) introduced significant updates, including the Scenario Model Intercomparison Project (ScenarioMIP) and the Shared Socioeconomic Pathways (SSPs) (Eyring et al., 2016). Indeed, it is an effort by the IPCC to incorporate socioeconomic and human-related factors into climate models, as emphasized in the IPCC's Sixth Assessment Report (AR6) (IPPC, 2021; Meyer, 2015). Specifically, SSPs detail future scenarios of greenhouse gas emissions and incorporate anthropogenic impacts as well as land use and land cover (LULC) under specific baseline storylines (Neill et al., 2016). By utilizing these scenarios in hydrological models, researchers can better understand the combined physical impacts of climate change and societal developments on hydrological processes. For this study, the NASA Earth Exchange Global Daily Downscaled Projections – NASA NEX-GDDP-CMIP6 is recommended, widely recognized for its application in previous works (Park et al., 2023; Saadi et al., 2024).

In this study, we aim to quantify the impacts of future climate on hydroclimatic extremes such as floods, droughts, and SLR for the ESVA. Our analysis incorporates different indices and approaches to assess projected vulnerabilities caused by climate change, considering different factors, e.g., regional demographics, changes in LULC, and coastal hazards. The results would provide valuable scientific basis to stakeholders and authorities in planning sustainable strategies and ensure human well-being. Besides, our findings will support the National Flood Insurance Program (NFIP) (FEMA, 2023a) launched by the Federal Emergency Management Agency (FEMA) in quantifying coastal risk through the nation's coastal Flood Insurance Studies (FIS) (FEMA, 2020a) and Flood Insurance Rate Maps (FIRMs, or flood maps) (FEMA, 2020b, 2023b). In addition, this study reveals the magnitude of projected future flood risk for towns and regions over ESVA, in which the newest release of the CMIP6 GCMs based on the IPCC AR6 and the IPCC's report on Ocean, Cryosphere, and Sea Level Change (IPCC, 2023) were used.

2. Materials and methods

2.1. Study area

ESVA is a coastal and risk-prone region which is located between the Atlantic Ocean and the Chesapeake Bay, with a length of approximately 110 km and a width ranging from 15 to 30 km (Fig. 1). This region covers Accomack and Northampton counties with a total area of 1764.43 km^2 (Sanford and Pope, 2010). The terrain of ESVA is predominantly flat, with elevations ranging from sea level to about 15 m above sea level, and is characterized by deep and sandy soils. The climate is classified as humid subtropical, marked by mild winters and warm, humid summers. Precipitation is evenly distributed throughout the year, with an annual average of 1143 mm (Sanford and Pope, 2007, 2010). The local economy is dependent on agriculture, fisheries, and tourism. Traditional farming practices in the area mainly involve the cultivation of corn, soybeans, and various small grains, which are crucial to regional agriculture.

Four important towns (S1–4) (Fig. 1c-f) have been highlighted in our analysis due to their significance in terms of economy, natural ecology, and human lives. Specifically, Melfa and Cape Charles serve as commercial hubs of the ESVA (Ralph and George Carrington, 1952), while Exmore is a populated town, and Accomac serves as the headquarters for many departments of Accomack County. As of the time of conducting this work, there are no current available observed streamflow data measured by USGS over the ESVA that could be used for hydrological model in terms of calibration and validation (2003–2020). This limitation can be attributed to the challenges in measuring streamflow data due to tidal and backwater effects, as well as the low elevation of this region (Andrews et al., 2019). Therefore, we have expanded our model area to include the state of Maryland (MD) (Fig. 1b) to obtain the necessary data (in Pocomoke and Nassawango Creek stations) (Fig. 1b). Within this study, the entire area will be referred to as MD-ESVA in our analysis, while ESVA will specifically represent the Eastern Shore of Virginia.

2.2. GCMs and SSP scenarios

To quantify the impacts of future projected extremes over ESVA, we employed the NASA NEX-GDDP-CMIP6 dataset, which offers downscaled and bias-corrected GCMs with a spatial resolution of 0.25° x 0.25° (approximately 25 × 25 km) (Thrasher et al., 2022). The datasets have been downscaled using the Bias-Correction Spatial Disaggregation (BCSD) method, a trend-preserving statistical downscaling algorithm, widely used to generate accurate and high-resolution data from GCMs (Maurer and Hidalgo, 2008; Wood et al., 2002, 2004).

Recent studies have found that the BCC-CSM2-MR, CanESM5, MIROC6, and MRI-ESM2–0 models demonstrate effective application in future climate investigations (Chen et al., 2022; Park et al., 2023; Peng et al., 2023; Thrasher et al., 2022; Nguyen et al., 2024). Consequently, these models have been chosen for our study due to their capabilities to comprehensively capture the high variability in future meteorological changes. Specifically, these four models have been shown to capture a broad range of changes in streamflow (Chen et al., 2022; Peng et al., 2023; Xu et al., 2023). Besides, Wang et al. (2021) highlighted that CanESM5 and BCC-CSM2-MR produce satisfactory results in terms of precipitation, evapotranspiration, and soil water. Furthermore, MIROC6 and MRI-ESM2–0 were found to have the highest adaptability in temperature and precipitation, surpassing the other GCMs (Peng et al., 2023). In this study, we have chosen the intermediate (SSP2–45) and high-end (SSP5–85) scenarios (Thrasher et al., 2022) for analysis. The summary of these selected GCMs can be found in Supplementary Table A1.

2.3. Hydrological SWAT model

SWAT is a semi-distributed hydrologic model developed by the United States Department of Agriculture (USDA) Agricultural Research Service (ARS) (Tran et al., 2022a). This model has been widely used in recent years for hydrological applications in watershed management (Ahmed et al., 2020; Tran et al., 2023c), focusing on the physical impacts of various factors on water regimes. These include the effects of climate change (Chen et al., 2022; Tran et al., 2023b, 2024a; Shafeeque et al., 2023), ecosystem services (Ashrafi et al., 2022), LULC changes (Cheng et al., 2018; Tran and Lakshmi, 2022), and the validation of satellite-based observations (Aryal et al., 2023; Tran et al., 2023a).

2.3.1. Study workflow and model setup

Fig. 2 presents the schematic workflow of our study, developed from Tran et al. (2024b) with additional details on the demographics and SLR data utilized for analysis of current and future impacts. Specifically, we aim to include in-depth assessments to determine the correlation between regional demographics, LULC changes, climate extremes, and

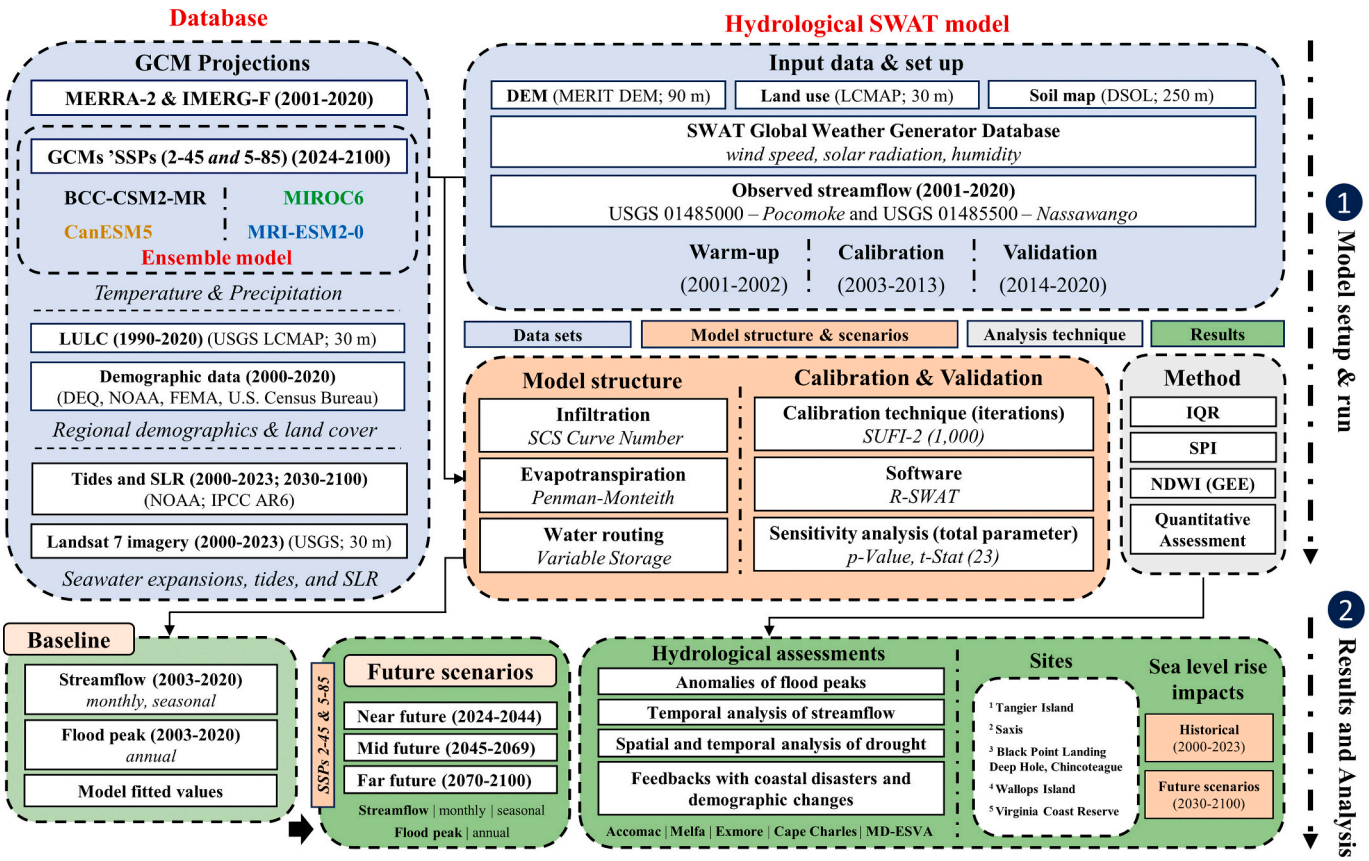

Fig. 2. The schematic flowchart used in this study. First, we prepared the necessary datasets for SWAT, which included the NASA Integrated Multi-satellitE Retrievals for Global Precipitation Measurement (GPM IMERG) V6.0 Final run (Hou et al., 2014) for daily precipitation and the Modern-Era Retrospective analysis for Research and Applications V2.0 (MERRA-2) (Gelaro et al., 2017) for daily temperature. The projected daily precipitation and temperature datasets (2024-2100) were extracted from CMIP6 GCMs for future scenarios (see section 2.2).

SLR. The SWAT model, operated using the Quantum Geographic Information System (QGIS) (V3.16.9) software, was used for the model run (Dile et al., 2019). Watershed delineation was performed using the Terrain Analysis Using Digital Elevation Models (TauDEM) version 5.0 (Tarboton, 2011).

For the SWAT model, we conducted watershed extraction and analyzed hydrologic information derived from the DEM input. This analysis was essential to delineate streams, sub-basins, and Hydrological Response Units (HRUs) (Arnold et al., 2012; Pignotti et al., 2017). The watershed was divided into smaller sub-watersheds, and the watershed characteristics from the DEM, combined with LULC and soil characteristics, were stored in HRUs. Specifically, HRU in SWAT represents the smallest spatial unit (Arnold et al., 2012), where the water balance equation is used for calculation.

In this study, we modified the common approach used in traditional SWAT models to better suit the unique characteristics of this region. Due to its low elevation, predominantly flat terrain, and small area (see section 2.1), the SWAT model first encounters difficulties in delineating stream networks and subbasins. This challenge commonly appears in coastal regions (Tran et al., 2023a) and can be explained due to the lack of steep slopes, with most regions in the study area having slopes below 5^{o} (Sanford and Pope, 2010). These characteristics limit our ability to accurately identify flow directions across the watershed. However, to address this, we tested seven different DEM products and selected the Multi-Error-Removed Improved-Terrain (MERIT) DEM (90 m) (Yamazaki et al., 2019), which provided the most accurate stream delineation over the MD-ESVA. The delineated stream network was validated using the survey network from the HydroRIVERS (Lehner and Grill, 2013) and Google Earth database to ensure the accuracy of our SWAT model set up.

On the other hand, LULC data from LCMAP (30 m) (1990–2020) (Fig. 3b) (USGS, 2020) and soil data from DSOLMap (250 m) (Fig. 3c) (Adrian et al., 2023) were extracted. To calibrate and validate the SWAT model, data from the USGS database (2003−2020) for the Pocomoke and Nassawango hydrological stations were used (Figs. 1b). The first two years (2001 and 2002) of this 20-year simulation period were chosen as the warm-up period. The calibration period was chosen between 2003 and 2013, with the validation period between 2014 and 2020 (Figs. 2 and 3). A total of 1000 iterations were performed along with 23 parameters were chosen for the model calibration and calibration on a daily scale using the interactive web-based application R-SWAT (Nguyen et al., 2022).

The historical scenarios were simulated for the period between 2003 and 2020, while future climate scenarios were catergorized as the near future (2024-2044), the mid future (2045–2069), and the far future (2070–2100) (Fig. 3d). These simulations utilized the calibrated parameters derived from the historical scenario (Fig. 2). The chosen parameters, fitted values, and their descriptions can be found in Supplementary Table A2.

2.4. Anomaly detection of future flood peaks

In this study, the IQR was used to detect anomaly flood events (2024–2100) by segmenting the dataset into quartiles, providing an overview of data distribution (Wan et al., 2014). Scenarios utilizing GCMs' meteorological inputs were performed, and the future flood peaks were collected for calculations. We defined the first quartile (Q1) as the median of the dataset's lower half and the third quartile (Q3) as the median of the dataset's upper half. Additionally, the second quartile

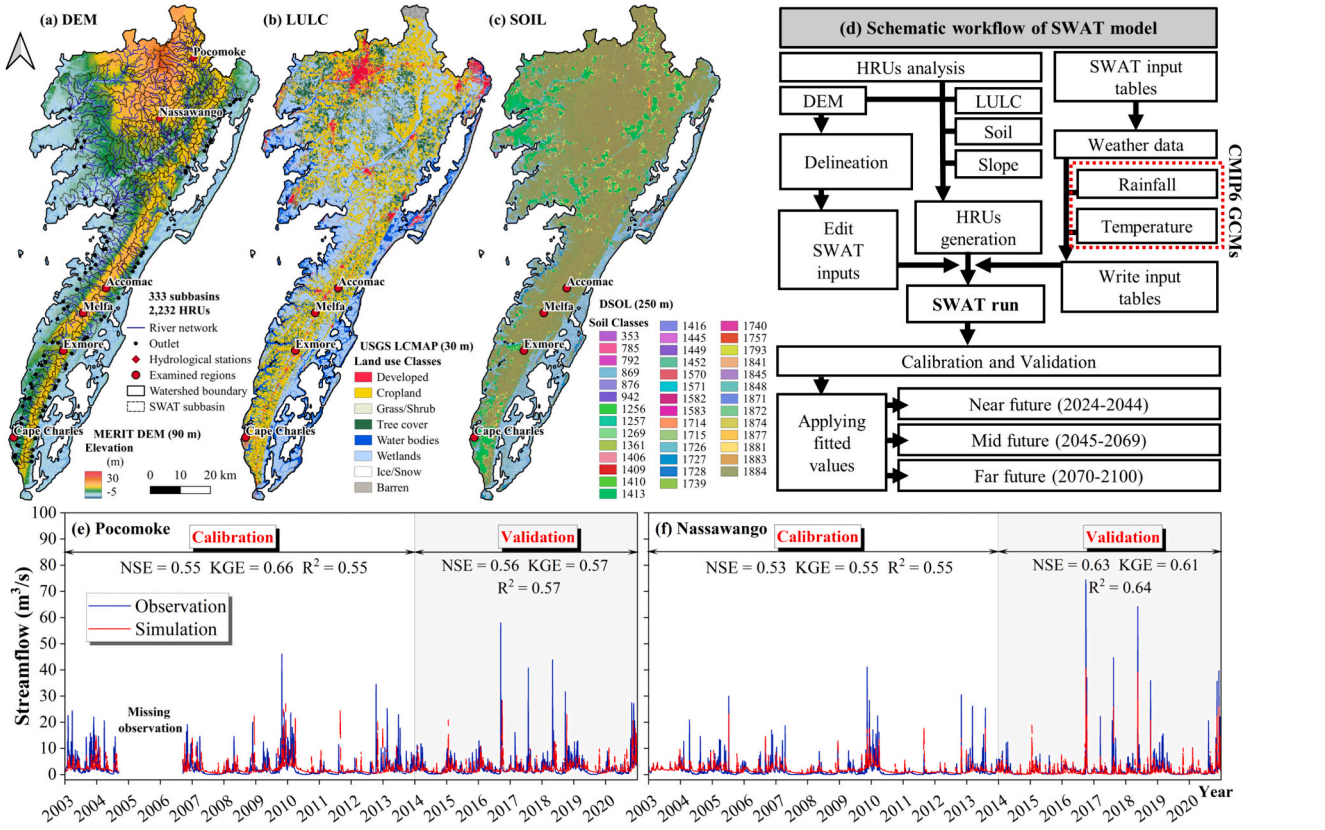

Fig. 3. Spatial representation of (a) DEM, (b) LULC, (c) Soil map, (d) Schematic workflow of the SWAT model, and model performance during calibration and validation shown for (e) Pocomoke station and (f) Nassawango station.

(Q2) was defined as the overall median of the dataset, while the IQR range was calculated as Q3 – Q1. The upper and lower bounds were calculated as (Q3 + (1.5 × IQR)) and (Q1 – (1.5 × IQR)), respectively. Peak values located outside these bounds were considered anomalies and used for further analysis.

2.5. Assessment of hydroclimatic extremes

To accurately assess climate extreme conditions, it is important to establish criteria for determining the duration of events, especially concerning the monitoring index used (Zhong et al., 2022). In our study, we employed the Standardized Precipitation Index (SPI) for analysis, with levels of drought severity indicated by the US Drought Monitor (Svoboda et al., 2002). Specifically, drought conditions are identified when the SPI values fall below zero and continue to decrease to less than negative one (−1). Conversely, a drought event or dry condition is considered to have ended when the SPI values return to positive, with wetter conditions identified when the SPI values move towards positive two (+2) and beyond. The description of this index, as well as the summary of severity categories with their ranges, can be found in Supplementary Table A3.

2.6. Coastal seawater expansion using NDWI

2.6.1. Landsat 7 data

In this study, to reveal the historical seawater expansion along the coast of ESVA from 2000 to 2023, we utilized the USGS Landsat 7 Collection 2 Tier 1 calibrated Top of Atmosphere (TOA) reflectance data obtained through the Google Earth Engine (GEE) platform (Gorelick et al., 2017; Nghia et al., 2022b). Additionally, the data undergone geometric correction based on ground control points, radiometric and atmospheric corrections, and was filtered for cloud coverage (≤ 10 %) before processed.

2.6.2. NDWI for seawater changes along the coast

The NDWI is used to monitor changes related to water content in water bodies. Since water bodies strongly absorb light in the visible to infrared electromagnetic spectrum, NDWI utilizes the green and near-infrared (NIR) bands to highlight water bodies. In this study, it is calculated using the surface reflectance of the Green (Band 2) and NIR (Band 4) wavelengths from Landsat 7, as specified below:

$$NDWI = \frac{Green - NIR}{Green + NIR} \quad (1)$$

The NDWI is designed to maximize the reflectance from water features by using green wavelengths, while minimizing the low reflectance from water in the NIR wavelengths and taking advantage of the high reflectance from vegetation and soil in NIR. Thus, water features exhibit positive values and are thus enhanced, whereas vegetation and soil typically display zero or negative values, and are therefore suppressed (Gao, 1996). Specifically, NDWI values range from −1 to +1 and are important for delineating water bodies using satellite imagery. In this study, the corresponding NDWI ranges are categorized as follows: water surface (0.3 to 1), flooding or wet conditions (0.0 to 0.3), moderate dryness or non-aqueous surfaces (−0.3 to 0.0), and dry or non-aqueous surfaces (−1 to −0.3) (McFeeters, 1996).

2.7. Performance metrics

In our study, we utilized the Kling-Gupta efficiency (KGE) (Gupta et al., 2009), Nash-Sutcliffe efficiency (NSE) (Nash and Sutcliffe, 1970), and Coefficient of determination (R^2) (Moriasi et al., 2015) for the evaluation of the SWAT model outputs. The specific ranges and equations of these metrics can be found in Supplementary Table A4.

3. Results

3.1. SWAT calibration and validation

The model calibration and validation on the daily scale for the period from 2003 to 2020 yielded acceptable results (Fig. 3e and f). In general, for the Pocomoke station, our model achieved a NSE score of 0.56, R^2 score of 0.56, KGE score of 0.62 (Fig. 3e) while they are 0.58, 0.61, and 0.58, respectively, for the Nassawango station (Fig. 3f). These results are categorized as Satisfactory (see Supplementary Table A4) which can be then used to investigate the impacts of climate change in the following sections.

3.2. Relationship between historical LULC, regional demographics, and climate extremes

When examining the correlation between demographics, LULC changes, and hydroclimatic extremes over ESVA, we found trends similar to those of the United States. Firstly, as the significant increase in the United States population between 2000 and 2010, explained by urbanization and increased crop needs (Bounoua et al., 2018), the population in ESVA has relatively increased (highest found at 16.75 % in Cape Charles; Fig. 1f) except Melfa with a small decrease of 2.70 % (Fig. 1d). Secondly, there was a significant increase in vacant residential units. Although a total population of 45,426 people was recorded in ESVA in 2022 (U.S. Census Bureau, 2022), there are around 10,083 vacant residential units, with only 5 % of them available for sale or rent (A-NPDC, 2022). We found that most of them are abandoned, dilapidated, condemned, and a staggering 56 % of unoccupied units have been

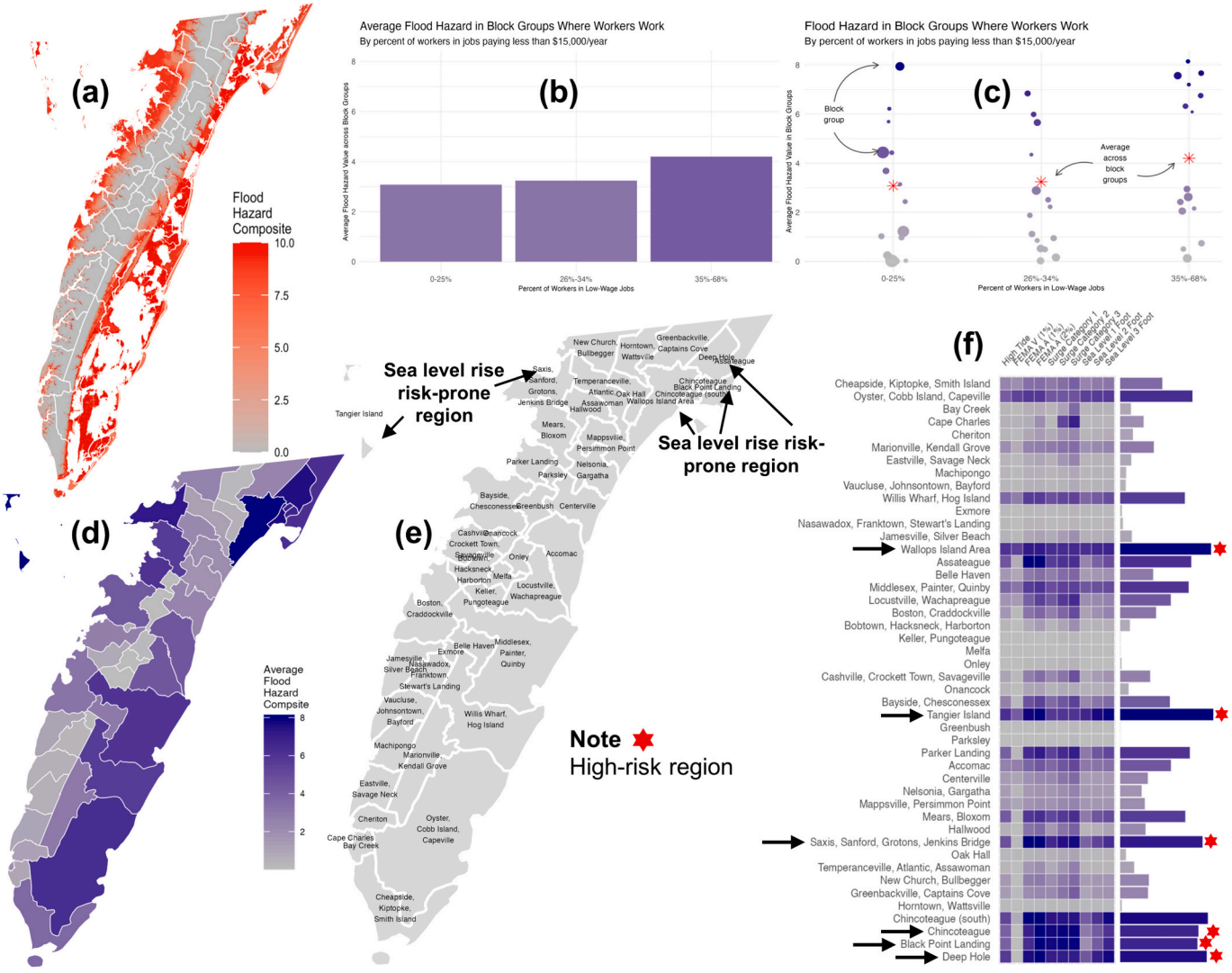

Fig. 4. Demographic changes and coastal hazard events including (a) coastal flood hazard composite, (b, c) average flood hazard in different income-block groups, (d) average inland flood hazard composite, (e) locations of towns over ESVA, and (f) summary of the risk-exposure benchmark over towns (Brideau et al., 2024). Hazard composite includes the most popular types of hazards, including high tide, storm surge, coastal flooding, and SLR. These included analyses of the following ten flood hazard zones: FEMA V zones, FEMA A zones, FEMA shaded X zones (FEMA, 2010), NOAA Office for Coastal Management (OCM) Flood Frequency zones, NOAA OCM potential SLR-induced inundation extents for 1 ft (0.3 m), 2 ft (0.6 m), and 3 ft (0.9 m) above current Mean Higher High Water (MHHW) (NOAA, 2024a), and Sea, Lake, and Overland Surges from Hurricanes (SLOSH) Maximum of the Maximums (MOMs) (NOAA, 2001) for categories 1, 2, and 3 hurricanes. Demographic and population data (e.g., race, age, home ownership/rental, online access, income, rent, home value, and housing age) were extracted from the American Community Survey 5-year estimates (U.S Census Bureau, 2023) while the low-wage workers (annual income around $15,000/year) by place of residence and by place of work are defined and provided by the Origin-Destination Employment Statistics (LODES) (U.S. Census Bureau, 2007), and the Longitudinal Employer-Household Dynamics (LEHD) (U.S. Census Bureau, 2010).

designated as vacation rentals. The lack of accommodation in good conditions for sale or rent leads to an increase in population density in urban and economically oriented areas such as S1-S4 (Fig. 1c-f). This trend, once highlighted by Wayne (2022), currently faces no regulatory prevention. Additionally, more densely populated areas have been proven to experience more climate-related risks, in which residents would encounter higher challenges in evacuation during extreme weather events (Lazo et al., 2015).

On the other hand, when examining the correlation between historical demographic changes and coastal hazards, we found that ESVA is highly susceptible to extreme events. Specifically, most coastal regions exhibited a high ratio of exposure to diverse types of extreme events, such as high tides, coastal flooding, and SLR (Fig. 4a) (FEMA, 2010). Inland regions and towns also suffered significant damage from storm surges and inundation, primarily due to their low elevation and geographic location (Fig. 1b) (see section 2.1) (Sanford and Pope, 2010). We also found that during climate extreme events, rainfall could not be drained into the Atlantic Ocean because of the differential in water pressure against the seawater. The Virginia Coast Reserve (VCR), a biosphere reserve created by The Nature Conservancy in the early 1970s, was found as highly vulnerable, mainly due to its low-lying topography and geographical location (Fig. 1b). Furthermore, the soil layers in ESVA were found to be highly saturated, with a high-water table elevation (Sanford and Pope, 2010), thereby retaining more water inland and exacerbating inundation issues (Fig. 4a and d).

Fig. 4b shows the flood hazard value for each block group, with the average values shown in Fig. 4c. We found that block groups with high flood hazard values are distributed across all levels of low-wage employment in ESVA. Additionally, block groups where >35 % of the jobs pay less than $15,000 per year exhibit higher flood hazard values (Fig. 4b and c). These low-income groups are more susceptible to coastal disasters, with a trend showing that more workers in low-wage jobs tend to experience a greater number of flood hazard events (Fig. 4b and c). We also summarized and ranked the vulnerability levels of towns in ESVA to historical coastal extremes in Fig. 4e and f. Six towns, including Tangier Island, Saxis, Wallops Island, Black Point Landing, Deep Hole, and Chincoteague, were indicated as most susceptible compared to others (Fig. 4f). These towns, along with VCR (Fig. 1b)—located along the ESVA coast—will be examined in sections 3.7 and 3.8 for historical and projected SLR scenarios.

Table 1
Projected difference (in percentage) in average monthly precipitation and temperature for the period (2024-2100) compared to the historical scenario (2003–2020). The darker color indicates higher changes. For temperature (T), the red color represents a higher increase compared to the blue color. For precipitation (P), the blue color indicates an increasing trend, whereas the red color signifies a decreasing trend. BCC is BCC-CSM2-MR, Can is CanESM5, MIR is MIROC6, and MRI is MRI-ESM2–0.

Max T	**Ensemble 2-45**	**Ensemble 5-85**	BCC 2-45	Can 2-45	MIROC 2-45	MRI 2-45	BCC 5-85	Can 5-85	MIROC 5-85	MRI 5-85
1	75.09	85.64	63.50	73.90	82.83	80.12	77.63	88.08	88.38	88.48
2	90.93	105.61	94.01	102.54	85.75	81.43	113.43	117.24	98.49	93.29
3	78.17	87.19	88.14	86.06	67.65	70.83	98.68	94.70	75.24	80.12
4	53.96	60.25	59.38	59.13	46.87	50.46	66.84	67.29	51.03	55.84
5	40.97	46.38	45.78	45.54	34.74	37.83	51.97	53.07	39.06	41.44
6	29.24	33.56	32.79	34.36	25.15	24.66	37.41	39.45	28.99	28.41
7	20.68	24.09	21.74	23.14	17.94	19.92	25.14	26.95	21.13	23.13
8	19.23	22.90	19.00	19.72	18.47	19.75	22.91	24.48	21.44	22.76
9	18.90	23.25	14.68	18.44	20.11	22.35	17.85	24.95	24.42	25.76
10	19.35	25.91	11.34	18.85	23.09	24.14	16.85	29.35	28.32	29.14
11	24.19	30.46	14.53	23.56	29.22	29.46	19.54	31.20	35.81	35.30
12	35.21	44.92	25.89	33.26	41.55	40.16	36.05	41.17	53.15	49.32
Min T	**Ensemble 2-45**	**Ensemble 5-85**	BCC 2-45	Can 2-45	MIROC 2-45	MRI 2-45	BCC 5-85	Can 5-85	MIROC 5-85	MRI 5-85
1	-33.18	18.52	-78.11	-9.82	-44.72	-0.06	-21.83	73.87	-17.94	39.96
2	37.53	97.97	33.63	107.12	-4.37	13.74	109.13	183.06	42.41	57.29
3	25.36	45.45	37.27	51.00	4.09	9.08	54.88	71.22	19.56	36.15
4	8.64	17.62	14.57	19.17	-3.45	4.29	22.62	29.45	3.70	14.71
5	4.00	10.61	6.61	10.43	-3.36	2.33	13.62	18.67	2.03	8.12
6	-1.80	4.04	0.33	3.53	-7.18	-3.86	5.19	10.60	-2.44	2.79
7	-4.93	-0.66	-4.77	-3.02	-7.30	-4.61	-0.74	2.74	-4.08	-0.55
8	-8.21	-3.58	-10.76	-8.43	-8.75	-4.92	-6.72	-2.09	-5.17	-0.32
9	-14.66	-8.73	-22.32	-14.28	-13.16	-8.89	-19.05	-5.02	-7.26	-3.57
10	-24.52	-15.20	-36.29	-22.26	-21.98	-17.54	-28.02	-6.11	-17.23	-9.44
11	-31.30	-20.42	-44.49	-24.83	-29.31	-26.58	-35.78	-8.02	-21.02	-16.88
12	-43.74	-20.44	-59.30	-36.91	-42.69	-36.05	-36.15	-8.21	-21.31	-16.09
P	**Ensemble 2-45**	**Ensemble 5-85**	BCC 2-45	Can 2-45	MIROC 2-45	MRI 2-45	BCC 5-85	Can 5-85	MIROC 5-85	MRI 5-85
1	8.94	10.18	6.13	5.67	0.96	22.99	9.80	8.30	13.52	9.09
2	9.00	18.48	19.44	14.01	-4.22	6.75	25.18	21.66	12.55	14.53
3	17.38	15.48	17.09	19.66	17.09	15.68	13.36	21.69	10.39	16.48
4	-2.78	-2.26	0.59	-4.57	-3.84	-3.28	-1.72	-5.04	4.60	-6.88
5	1.40	-0.26	-4.41	1.61	10.57	-2.16	-8.24	-3.20	10.11	0.30
6	-1.65	-2.90	-10.52	-0.24	-5.64	-6.18	-11.27	4.30	-11.56	-1.05
7	7.50	9.66	-10.80	17.30	9.92	13.58	-2.46	25.83	9.26	5.99
8	-1.47	1.61	-9.89	0.87	4.13	-0.99	-6.69	1.65	-0.34	11.84
9	0.83	3.91	-7.59	3.17	6.43	1.31	-4.39	3.95	1.96	14.14
10	1.82	4.22	0.89	-7.73	9.68	4.45	11.39	-5.22	8.90	1.80
11	-3.43	-2.72	-6.59	-19.00	-7.44	-20.70	1.54	-22.31	-19.31	-10.81
12	12.55	13.87	20.19	6.01	4.13	19.89	24.62	18.52	1.46	10.88

3.3. Projected changes in temperature and precipitation

First, we examined changes in average monthly temperature and precipitation across GCMs and SSPs (Table 1). The average monthly historical precipitation (2003–2020) was approximately 3.52 mm. However, this figure increases by 4.17 % to 3.67 mm under the SSP2–45 and to 3.73 mm under the SSP5–85 scenario between 2024 and 2100.

Table 1 shows notable trends in maximum and minimum temperatures, along with precipitation variations, across different GCMs and SSPs (2024-2100). For temperature, ESVA is projected to experience higher temperatures at the beginning of the year, with February and March identified as experiencing the most significant increases. Interestingly, a shift towards cooler weather is anticipated starting in August, highlighting a division between warmer and cooler seasons as we approach the year 2100. These results indicate an extreme trend in climate over ESVA, characterized by higher contrasts between hot and cold periods. For precipitation, an increase is observed as similar as the rise in temperatures, particularly from January to March while lowest precipitation is projected starting from April to November. This correlation suggests a potential for more pronounced seasonal extremes in ESVA.

3.4. Projected flood peaks

Flood peak is an important result from numerical models that is essential for hydrological assessment (Merz et al., 2022). Fig. 5 shows the projected flood peaks (a) Accomac, (b) Melfa, (c) Exmore, and (d) Cape Charles over future periods (2024-2100) under SSPs 2–45 and 5–85.

In general, we found that the number of high flood peaks increases starting from the mid-future period (2045–2069) across various regions compared to the near future (2024-2044) (Fig. 5). While projected flood peaks in the near future (2024-2044) remain relatively unchanged compared to the historical period, a higher number of record-breaking peaks are frequently observed in the mid and far future, with the more severe greenhouse gas emission pathway (SSP5–85) showing higher peaks compared to SSP2–45. Specifically, when comparing future projected flood peaks towards 2100 with historical flood peaks (2003–2020), we observed increases ranging from 3.41 to 8.65 % during the mid-future and up to 8.9 % during the far future across examined regions (Fig. 5). Additionally, we found that Exmore is the most susceptible to future flood peaks, followed by Melfa (projected peaks increase from 4.68 % in the mid-future to 5.84 % in the far-future), Cape Charles (4.27 % to 5.34 %), and Accomac (3.41 % to 4.32 %), respectively.

Anomaly flood peaks are key indicators of detecting potential risks in hydrological cycles, with significant implications for ecosystems and human communities (Maurer et al., 2018; Villarini and Smith, 2010; Yin et al., 2009). We employed the IQR method (see section 2.4) to identify projected flood peaks under various GCMs and SSPs for the near future (2024-2044), mid future (2045–2069), and far future (2070–2100) over the Accomac, Melfa, Exmore, and Cape Charles regions. In general, there is an increasing trend in the variability of flood peaks from the near to the far future, with the most significant peaks occurring under the SSP5–85 scenario, showing a correlation with higher emission pathway.

We found that the two populated towns, Exmore and Cape Charles, are projected to experience higher numbers of anomaly flood peaks starting from the mid-future, followed by Melfa and Accomac (Figs. 1 and 5). During the mid-future period (2045–2069), the year 2059 stands out due to its severity, with significant flood peaks found across these four towns. This is followed by 2056, with noticeable projected peaks found in Melfa and Cape Charles; 2050, for Exmore and Melfa; and 2048, for Cape Charles. During the far future, the year 2080 stands out for Exmore, which is projected to have an exceptionally high peak of 12.04 m^3/s, found as the highest among the years in this period, considering its relatively small area (Fig. 1e). Consistent with the presented results, we observed an increase in flood vulnerability for more populated towns with higher housing units, specifically Exmore and Cape Charles (Fig. 1). This presents a potential challenge for evacuation during extreme weather events. The increased vulnerability can be explained by the higher impervious surface coverage in developed areas, which prevents water from infiltrating into the ground, exacerbating runoff and flooding issues.

3.5. Seasonal streamflow changes

Fig. 6 shows the average monthly streamflow differences between the historical period (2003–2020) and the near future (2024-2044), mid-future (2045–2069), and far future (2070–2100). In general, these towns experience an increase in streamflow during the winter months (November to March), leading to a wetter condition (Fig. 6). Conversely, the period from April to July is projected to be the driest, with a significant decrease in streamflow compared to the historical period. Notably, these changes between wet and dry seasons are substantial, which could result in severe environmental issues, particularly for important towns such as Accomac, where the majority of Accomack County's administrative offices are located. As we approach 2100, the discrepancy in streamflow between wet and dry months is projected to exacerbate, especially under the higher emission scenario (SSP5–85). Additionally, wet months could become considerably wetter, while dry months show a substantial decrease in streamflow.

3.6. Temporal and spatial variations in climate extremes

In the previous section, we evaluated projected flood peaks for the period 2024–2100. However, quantifying these climate extremes both statistically and spatially is crucial. In this section, we employ the 12-month SPI index (see section 2.5) to assess the intensity and frequency of flood and drought events towards 2100. Fig. 7 and Table 2 show the magnitudes of these events for the ESVA and the four chosen towns (Fig. 1). In general, a drying trend is observed in the near-future period (2024-2044), as indicated by negative values (Fig. 7) while the entire ESVA is projected to experience wetter conditions during the mid- and far-future periods.

During the near future (2024-2044), ESVA region exhibits dry conditions ($\overline{SPI12_{near}^{2-45}} = -0.359$), then transitions to mild-wet conditions during the mid future (2044–2069) ($\overline{SPI12_{mid}^{2-45}} = +0.027$), and reaches its peak wetness in the far future ($\overline{SPI12_{far}^{2-45}} = +0.227$) (Fig. 7 and Table 2). This trend, indicating a shift from drier to wetter conditions, is found to occur across the examined regions and is projected to intensify under the impacts of SSP5–85. Specifically, the driest conditions are forecasted under SSP5–85 with ($\overline{SPI12_{near}^{5-85}} = -0.535$), while a substantially wetter condition is indicated for the far future ($\overline{SPI12_{far}^{5-85}} = +0.317$) (Table 2). Similarly, the four examined towns show similar trends compared to the ESVA. These results confirm our findings in previous sections, which suggest that (a) except for the dry conditions up to 2044, there is a general trend towards wetter conditions by 2100, starting from the mid-future period (2045–2069) while (b) higher emission projection (SSP5–85) is found to have more substantial impacts.

Fig. 8 shows the spatial representation of drought intensity and the probability of drought occurrences using SPI values calculated based on the ensemble model for MD-ESVA region. In general, drought has been identified as the major trend in the near future (2024-2044), with higher emission levels show higher severity. Locals in ESVA confirmed recent moderate drought events starting from 2020s in ESVA during the 2024 ESVA Climate Equity Workshop in Melfa, Virginia (Brideau et al., 2024) as well as in the July 2020 report by NOAA (NOAA, 2020). Furthermore, the Virginia Department of Environmental Quality (DEQ) recently placed ESVA on their drought watch advisory list (DEQ, 2024) due to increasing dry and drought conditions. These findings align with our

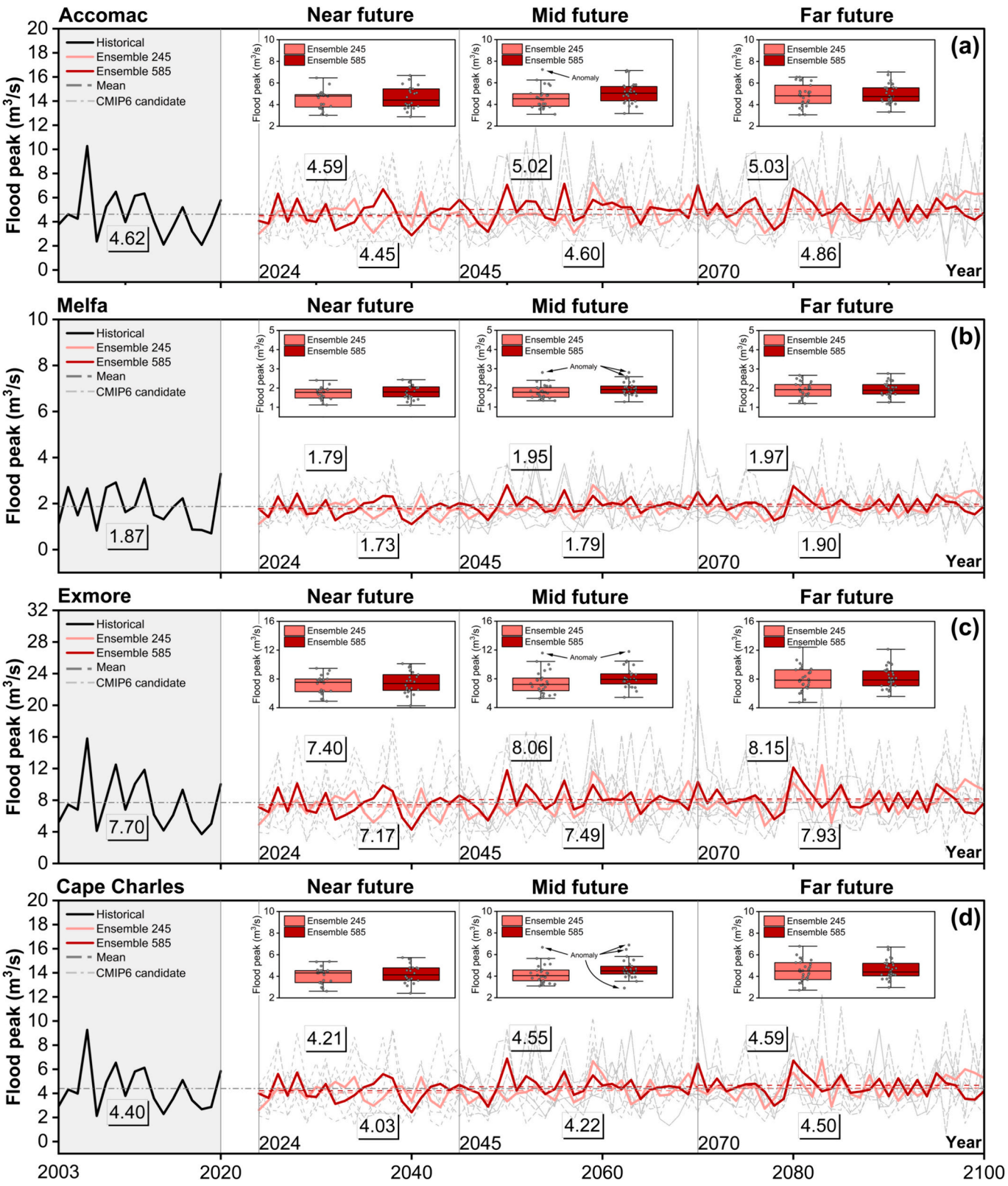

Fig. 5. Historical and projected flood peaks at (a) Accomac, (b) Melfa, (c) Exmore, and (d) Cape Charles. Future projections are simulated using the SWAT model, incorporating inputs from GCMs under different SSP scenarios (2–45 and 5–85). Black lines represent historical flood peaks (2003–2020), red lines represent the ensemble model (2024-2100), which combines the inputs from GCM candidates, while dash grey lines show the projections from individual GCMs. Values in boxes represent mean flood peaks over different future periods (near, mid, and far) and the box plots show the distribution of flood peaks from the ensemble model in which anomaly peaks were detected using the IQR method.

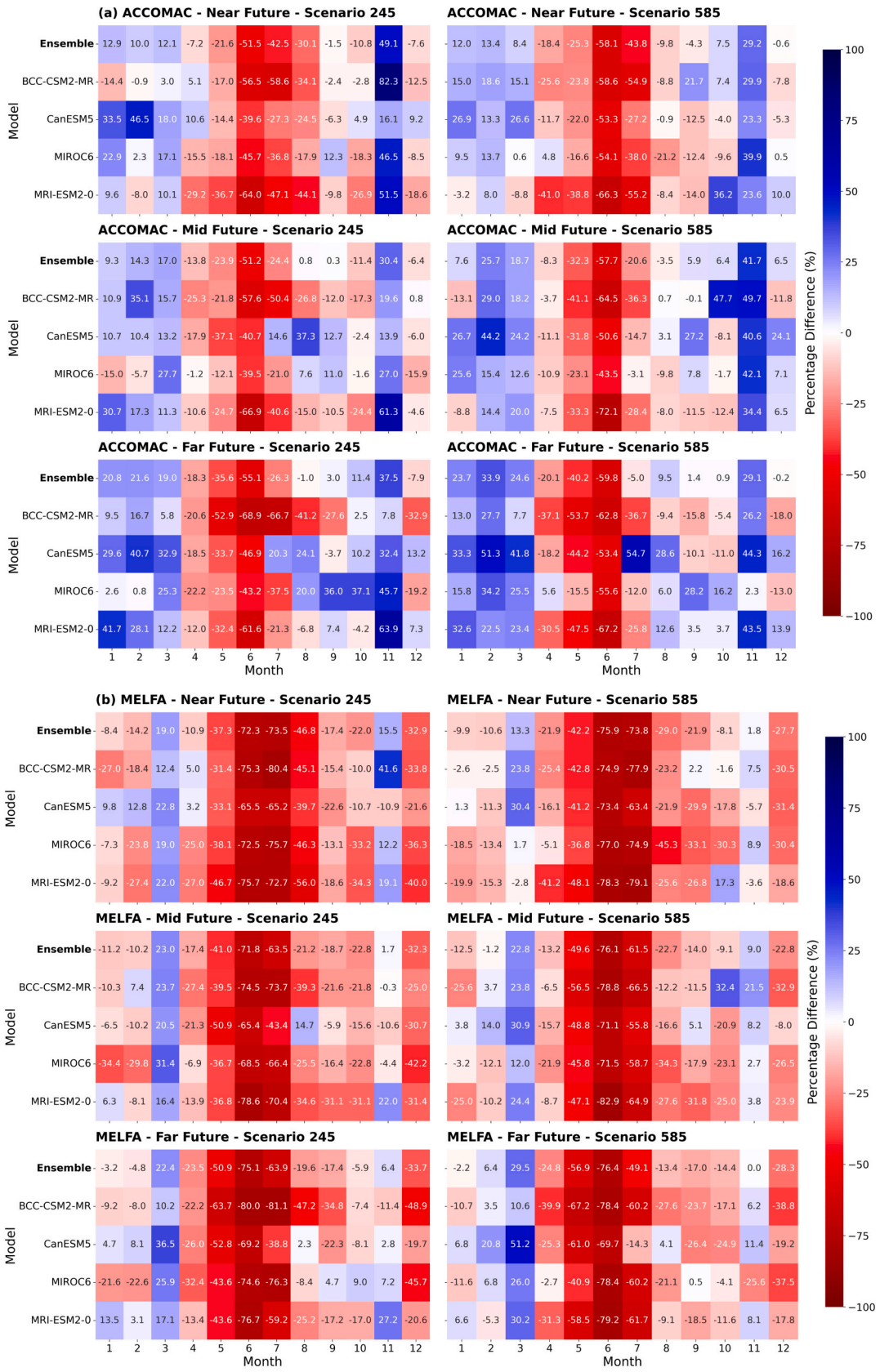

Fig. 6. The average monthly streamflow difference in percentage between the historical data, GCMs, and ensemble model in (a) Accomac, (b) Melfa, (c) Exmore, and (d) Cape Charles over the near future (2024-2044), mid future (2045–2069), and far future (2070–2100) under the SPP2–45 and 5–85 scenarios.

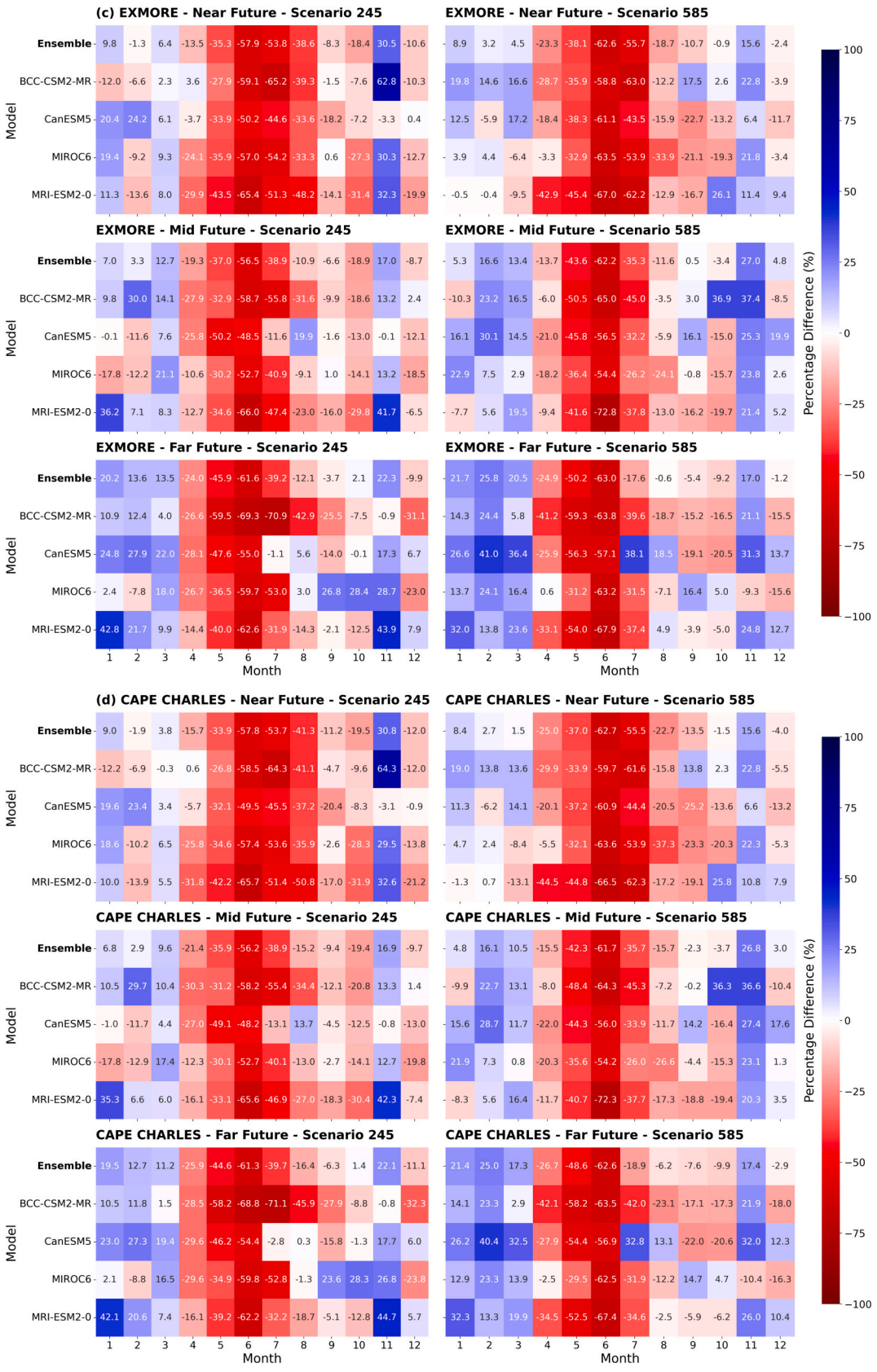

Fig. 6. (*continued*).

observations of current drying trends.

We found that ESVA is projected to become wetter towards 2100, reaching peak records during the far future, while the early period (2024-2044) is expected to exhibit dry conditions (Fig. 8c) and a higher occurrence probability of drought events, with the higher emission scenario indicating more severe impacts (Fig. 8d). Specifically, we found

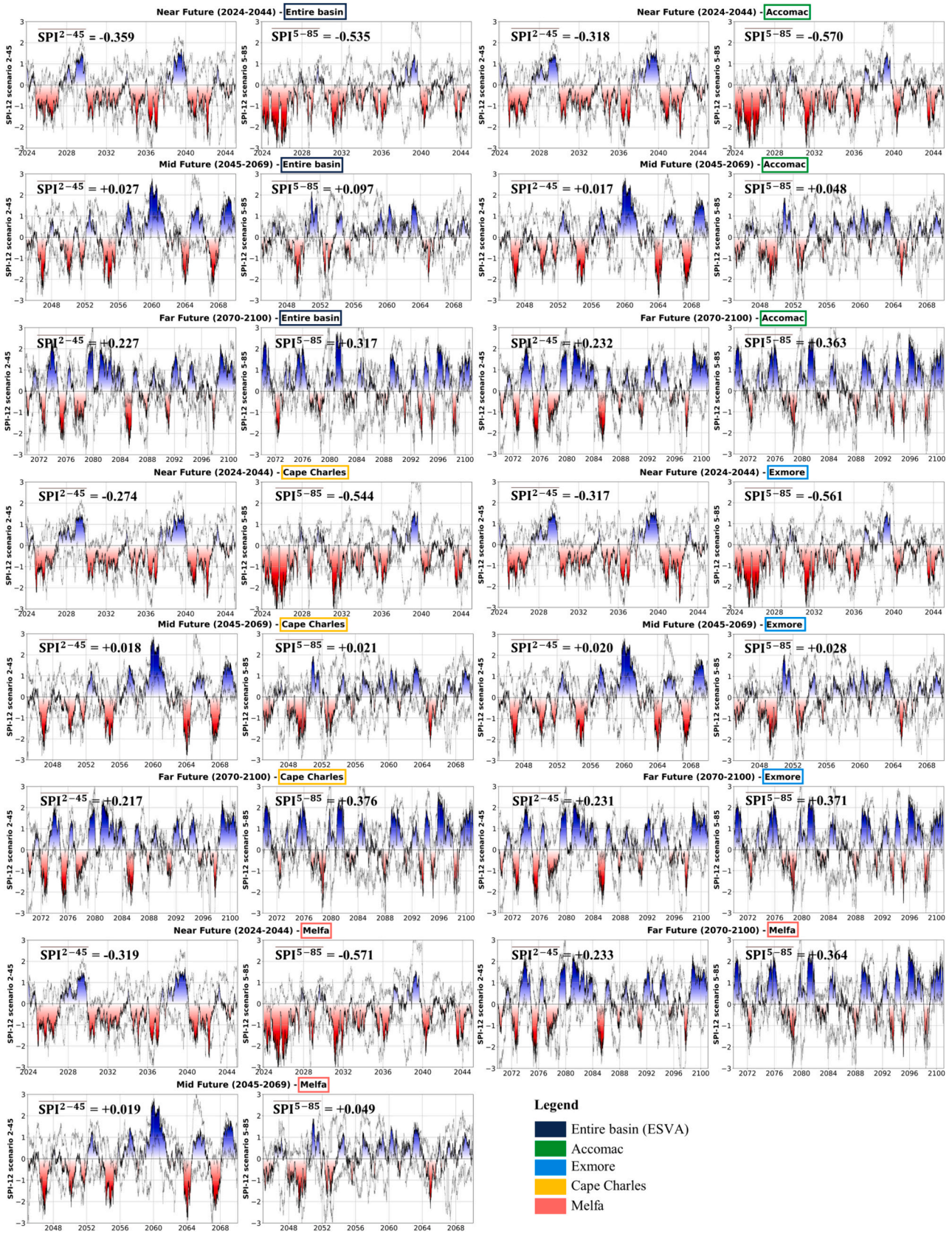

Fig. 7. Evaluation of drought and flood events using SPI-12 index for the (a) near future (2024-2044), (b) mid future (2045–2069), and (c) far future (2070–2100) under SSP2–45 and 5–85 scenarios. The red color indicates dry periods, while the blue color signifies wet periods using ensemble model. The severity classification of climate extremes can be found in Supplementary Table A3. The black dotted line represents the SPI ranges across different GCMs.

Table 2
Summary of the average SPI index for the Accomac, Melfa, Exmore, Cape Charles, and ESVA using the ensemble model across the near future (2024-2044), mid future (2045–2069), and far future (2070–2100). Positive (+) values, indicated in red, suggest a wet trend, while negative (−) values, shown in blue, denote a dry trend. The ranges for the SPI drought index can be found Supplementary Table A3.

Site	Ensemble model (SSP2-45)		
	Near future (2024-2044)	Mid future (2045-2069)	Far future (2070-2100)
Accomac	− 0.318	+ 0.017	+ 0.232
Melfa	− 0.319	+ 0.019	+ 0.233
Exmore	− 0.317	+ 0.020	+ 0.231
Cape Charles	− 0.274	+ 0.018	+ 0.217
ESVA	− 0.359	+ 0.027	+ 0.227
	Ensemble model (SSP5-85)		
	Near future (2024-2044)	Mid future (2045-2069)	Far future (2070-2100)
Accomac	− 0.570	+ 0.048	+ 0.363
Melfa	− 0.571	+ 0.049	+ 0.364
Exmore	− 0.561	+ 0.028	+ 0.371
Cape Charles	− 0.544	+ 0.021	+ 0.376
ESVA	− 0.535	+ 0.097	+ 0.317

that the highest drought occurrence around under 25 % in the near future, whereas it is found to be higher under the SSP5–85 scenario. However, these figures are projected to decrease towards the mid- and far-future periods as ESVA becomes wetter (Fig. 8d).

3.7. Historical seawater expansions, tides, and SLR

Mean Sea Level (MSL, also known as sea level) is an average surface level of one or more among Earth's coastal bodies of water from which heights such as elevation may be measured. According to Climate Change Service (C3S), European Centre for Medium-Range Weather Forecasts (ECMWF), and World Glacier Monitoring Service (WGMS), ice loss accounts for around 8226 gigatonnes (Gt) of water since 1976, of which 8100 Gt has been lost since 1991, and 3600 Gt since 2014 (C3S, 2024). The year 2023 was recorded as the warmest year since global records began in 1850 at 1.18 °C above the 20th-century average of 13.9 °C (NOAA, 2024b). This marked the considerable ice lost from glaciers globally that was equivalent to 1.7 mm of SLR and this is approximately 4.6 times the amount of ice contained in all glaciers in the European Alps (Farinotti et al., 2019). SLR arises from processes operating across a range of spatial and temporal scales involving the ocean, cryosphere, solid Earth, atmosphere, and land (IPCC, 2023). Since 1993, the global SLR observed an average increase of about 3.4 mm, particularly since 2000 (Hugonnet et al., 2021).

We first examine the historical seawater expansion along the coast of ESVA between 2000 and 2023 using NDWI (see section 2.6.2) (Fig. 9). Additionally, we present historical SLR and tide level provided by NOAA (NOAA, 2010) at four tidewatch stations: Chesapeake Bay Bridge Tunnel (CBBT; Virginia), Wachapreague (WACH; Virginia), Kiptopeke (KIPT; Virginia), and Ocean City Inlet (OCI; Maryland) (Fig. 9c). These stations are primarily located along the ESVA in Virginia (VA), except for the Ocean City Inlet, which is located in Maryland (MD). In this section, we also investigate the VCR region along with six disaster-vulnerable regions (Fig. 9a and b) due to their high susceptibility to coastal natural hazards and ecological significance to ESVA, identified using historical demographic data and coastal hazard events (see section 3.2).

In general, there is a noticeable increase in seawater expansion due to SLR from 2000 to 2023 along the coast of ESVA and significantly in the VCR, particularly in the Wallops Island, Deep Hole, Chincoteague, and Black Point Landing regions (Fig. 9a and b). This trend was also statistically observed using records from tidewatch stations during this period, where MSL, which is the average height of the sea's surface, showed significant increasing trends. Similarly, the MHW, the mean of all the high-water heights observed over the National Tidal Datum Epoch (NTDE), and the MLW, the mean of all low-water heights observed during the current NTDE, also showed significant increasing trends (p-value < 0.05) (Fig. 9c). Moreover, many parts of the four examined regions were shown to be submerged by seawater as detected in the year 2023. This situation is likely to worsen under future climate scenarios, which will be then discussed in the following section.

3.8. Projected SLR towards 2100

In the previous section, we discussed the historical seawater expansion caused by SLR over ESVA. However, it is important to understand this severe phenomenon for future context, in which we would investigate the projected SLR up to 2100 in this section. Specifically, we quantify the SLR magnitude under the SSP2–45 (mean global temperature increase of 3 °C) and SSP5–85 (mean global temperature increase of 5 °C) scenarios (IPCC, 2021, 2023) across the coast of ESVA, including (1) Tangier, (2) Saxis, (3) Wallops Island, (4) Deep Hole, Chincoteague, and Black Point Landing, and the VCR region (Fig. 10), which were identified as vulnerable due to natural hazards in section 3.2.

SLR is influenced by processes that operate across a range of spatial and temporal scales involving the ocean, cryosphere, solid Earth, atmosphere, and land (IPCC, 2023). This results from both global and regional processes, including thermosteric sea level change (also known as thermal expansion) and the melting of the Greenland and Antarctic ice sheets. In this work, we used the projected SLR for two greenhouse gas emission levels (SSPs 2–45 and 5–85) provided in the latest IPCC report on Ocean, Cryosphere, and Sea Level Change (IPCC, 2023). Specifically, these projections were extracted from the global mean sea level (GMSL) projections, which are derived from the independent contributions of land-water storage (e.g., surface water, soil moisture, groundwater storage, snow), ocean dynamic sea level change, alterations in Earth's gravity and rotation, viscoelastic solid Earth deformation, glacial isostatic adjustment, vertical land motion, and extreme sea level events (IPCC, 2023). These projections were updated using CMIP6 models to project the ocean dynamic sea level contribution to relative sea level (RSL) change, updating the previous findings from the IPCC Assessment Report 5 (AR5). In this work, the newly defined SLR projections under SSP2–45 based on the IPCC report on Ocean, Cryosphere, and Sea Level Change (IPCC, 2023) are projected as an increase of 0.09 m by 2030, 0.20 m (2050), 0.48 m (2090), and 0.56 m (2100), while under SSP5–85, they are 0.10 m (2030), 0.23 m (2050), 0.63 m (2090), and 0.77 m (2100) (Fig. 10). These projections will be combined with the baseline scenario analyzed for the year 2023 (see section 3.7) to provide a continuous analysis of future SLR impacts on this region.

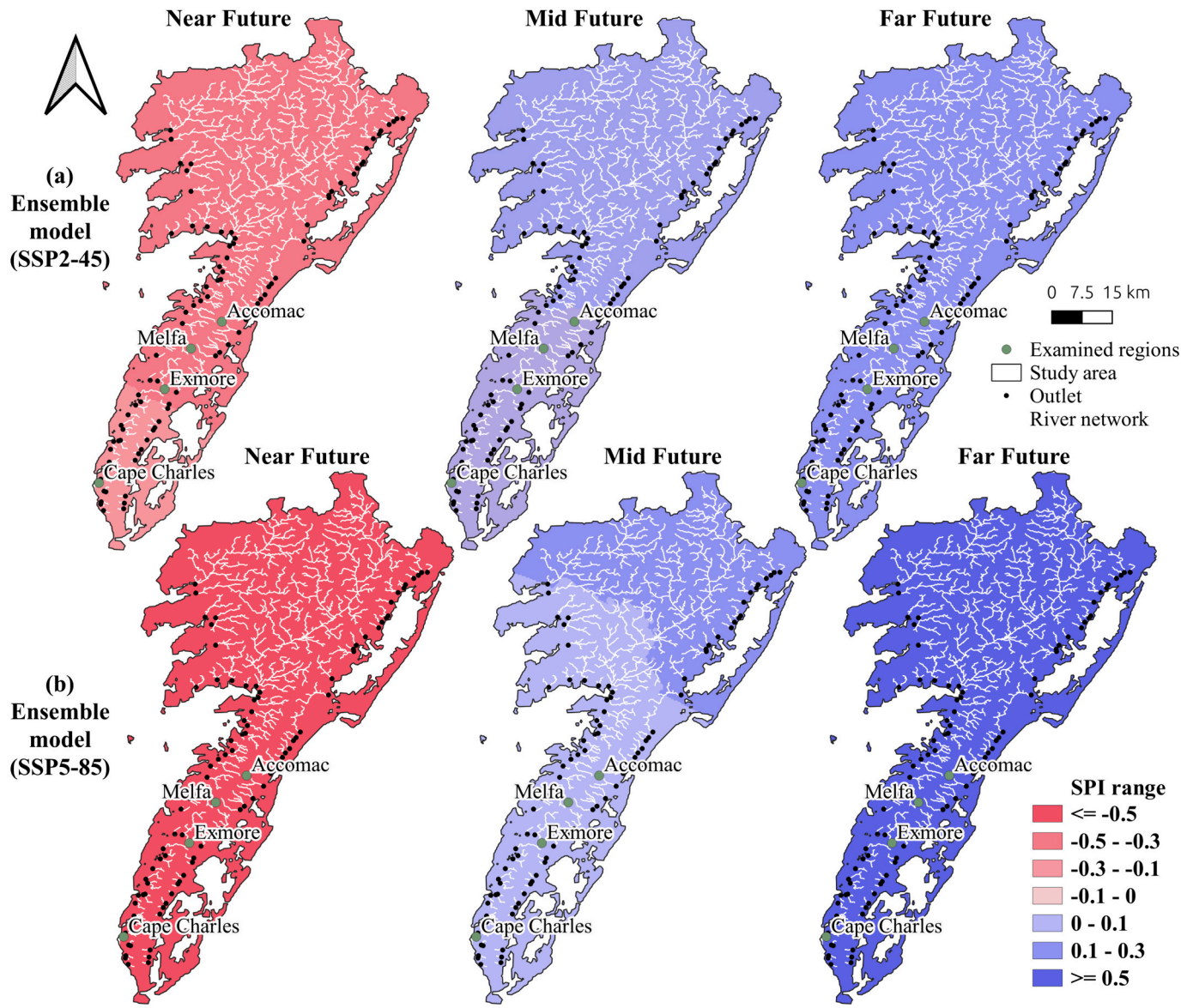

Fig. 8. Spatial distribution of drought intensity and occurrence probability using SPI index over different GCMs and the ensemble model within future periods, including near future (2024-2044), mid future (2045–2069), and far future (2070–2100). For (a-b), the blue color represents the wet trend while the red color represents the dry trend. For (c-d), different shades of yellow and grey are used to present the occurrence probability of drought in percentage. Darker colors represent higher severity.

Our findings indicate that projections for the years 2030, 2050, 2090, and 2100 reveal an escalating increase in SLR across ESVA and all examined regions, with a particularly notable intensification under the higher emission scenario (SSP5–85). We found that Tangier, Saxis, and Wallops Island are likely to be entirely submerged by future seawater due to their low elevations, while many parts of the Deep Hole, Chincoteague, and Black Point Landing regions are projected to be highly inundated by seawater by 2100 (Fig. 10b). Additionally, we observed that coastal regions and the VCR region are highly susceptible to SLR, with most of the areas along the VCR coast expected to be submerged by rising seawater (Fig. 10a). In general, the rising sea levels underscore a severe threat to the safety of current coastal ecosystems and human lives over ESVA, where saltwater intrusion and coastal erosion are likely to become more exacerbated due to SLR. This trend highlights the urgent need for strategic planning and adaptation measures to combat SLR-induced inundation, which could exacerbate the decline of farmland, contamination of groundwater by saltwater, reduction in living areas, and ecological imbalances in the ESVA region.

4. Discussion and suggestions

First, we found an increase in both total population and population density in examined towns between 2000 and 2020, despite a slight decrease in the total population across the entire ESVA (Fig. 1; see section 3.2). This indicates that people tend to reside in populated towns and regions in recent years, resulting in a marked increase in the total number of housing units, especially between 2010 and 2020 (Fig. 1). Furthermore, by 2050, it is projected that 89 % of the U.S. population will reside in urban areas (UN Population Division, 2018), and this trend is also highlighted at the state level. Our findings indicate that an increasing number of people are moving to developed areas with higher populations (see section 3.2), driven by (1) the aim of having higher salaries and (2) the deterioration of accommodations mainly caused by inland and coastal flooding (A-NPDC, 2022; Russ, 2020). The rise in

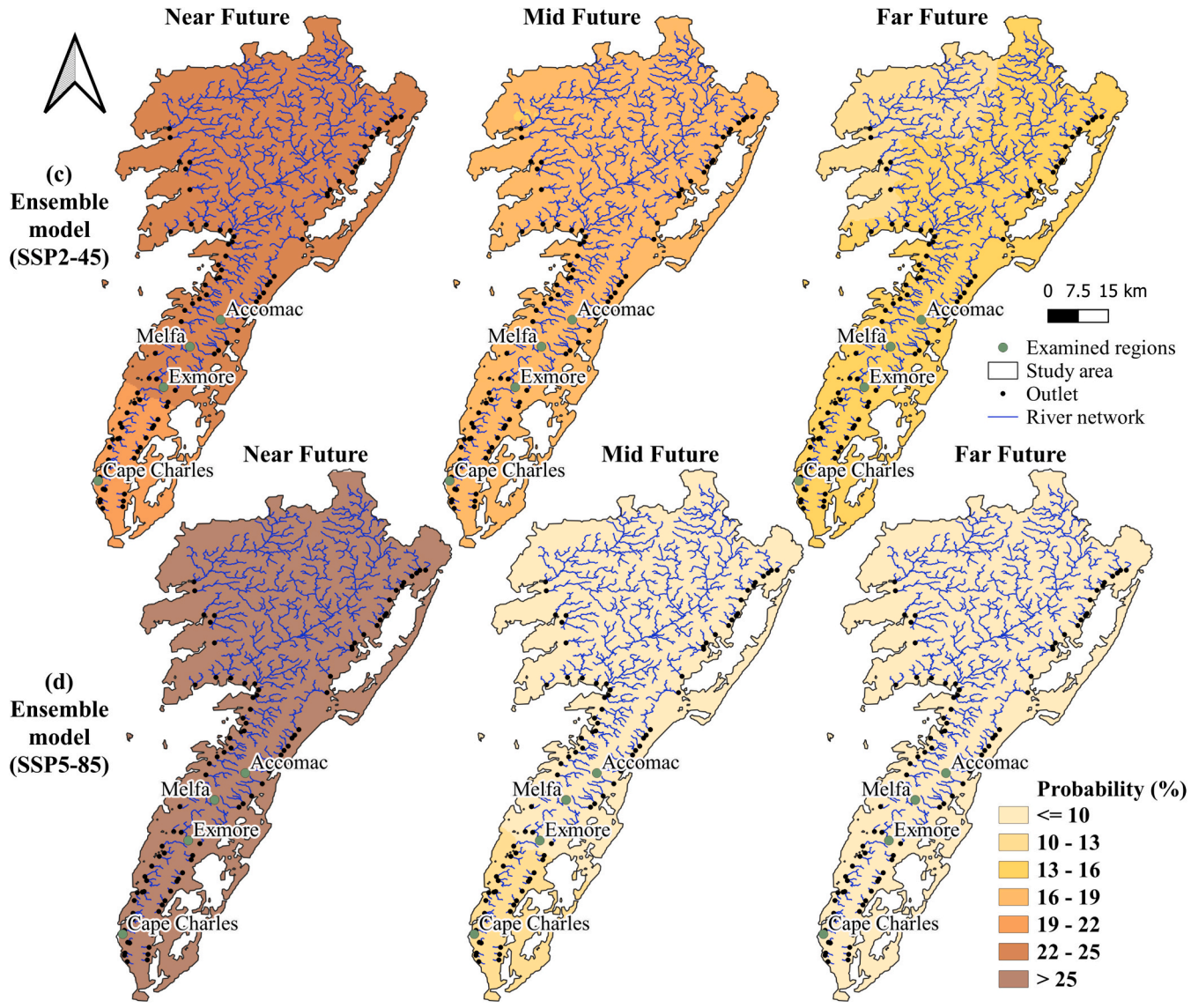

Fig. 8. (*continued*).

high-population regions leads to the development of new infrastructures for accommodation and public services (as shown in our current trend between 2010 and 2020) (Fig. 1), which could have several consequences, including an increase in urban heat (Chen et al., 2021; Yin et al., 2018; Zhang et al., 2013). On the other hand, the increase in housing units and concrete-based infrastructure significantly increases the total impervious surface area (Zhang et al., 2013), resulting in higher urban heat records (Nguyen et al., 2022b; Yin et al., 2018; Zhou and Chen, 2018). This phenomenon could profoundly impact socioeconomic conditions and human well-being, as explained by the increase in heat stress (Oleson et al., 2015), leading to heat-related illnesses (Chen et al., 2021). It is worth noting that the near future is expected to experience more severe impacts from drought, whereas the mid- and far-future periods are likely to see increased flooding impacts (see sections 3.5 and 3.6). This is similar to recent findings for the coastal Tar-Pamlico River basin (North Carolina), where the region is found to be dominated by floods, especially more severe in low-lying areas (Tran et al., 2024b). Besides, the driest months (April to July), especially during the near future (Table 6), could then increase the region's vulnerability to extreme heat and affect human lives, agricultural activities, and businesses. Furthermore, the continued rise in temperature towards 2100 (Table 1) could diminish economic productivity, particularly in physically demanding occupations (Kjellstrom et al., 2009), and discourage outdoor activities such as shopping and dining, thus affecting businesses reliant on foot traffic (Hoehne et al., 2018). Conversely, the far future is predicted to be highly prone to flooding (Fig. 8 and Table 2), which could cause more water-related issues in terms of water sanitation and hygiene.

Furthermore, ESVA is likely to face more challenges due to the rise in both unoccupied and vacant residential units. This concern, highlighted in our analysis (see section 3.2), comes with considerable implications. First, a substantial number of homes across ESVA are reported to suffer from a significant lack of indoor plumbing (Skeo, 2015). A report in 2014 by the U.S. Fish and Wildlife Foundation revealed that out of 1226 houses, 112 (approximately 9 %) lacked complete indoor plumbing facilities (A-NPDC, 2022). It is important to recognize that these homes pose a risk as sources of human waste disposal, potentially exacerbating uncontrolled pollution due to insufficient management efforts. The increasing population density may intensify this issue, leading to more polluted water and materials being discharged into the ground, affecting groundwater quality. Furthermore, ESVA is known for its abundant groundwater resources (Sanford and Pope, 2010), which complicates the task of mitigating pollution once contamination occurs. Our findings indicate a trend towards wetter conditions with increased inland

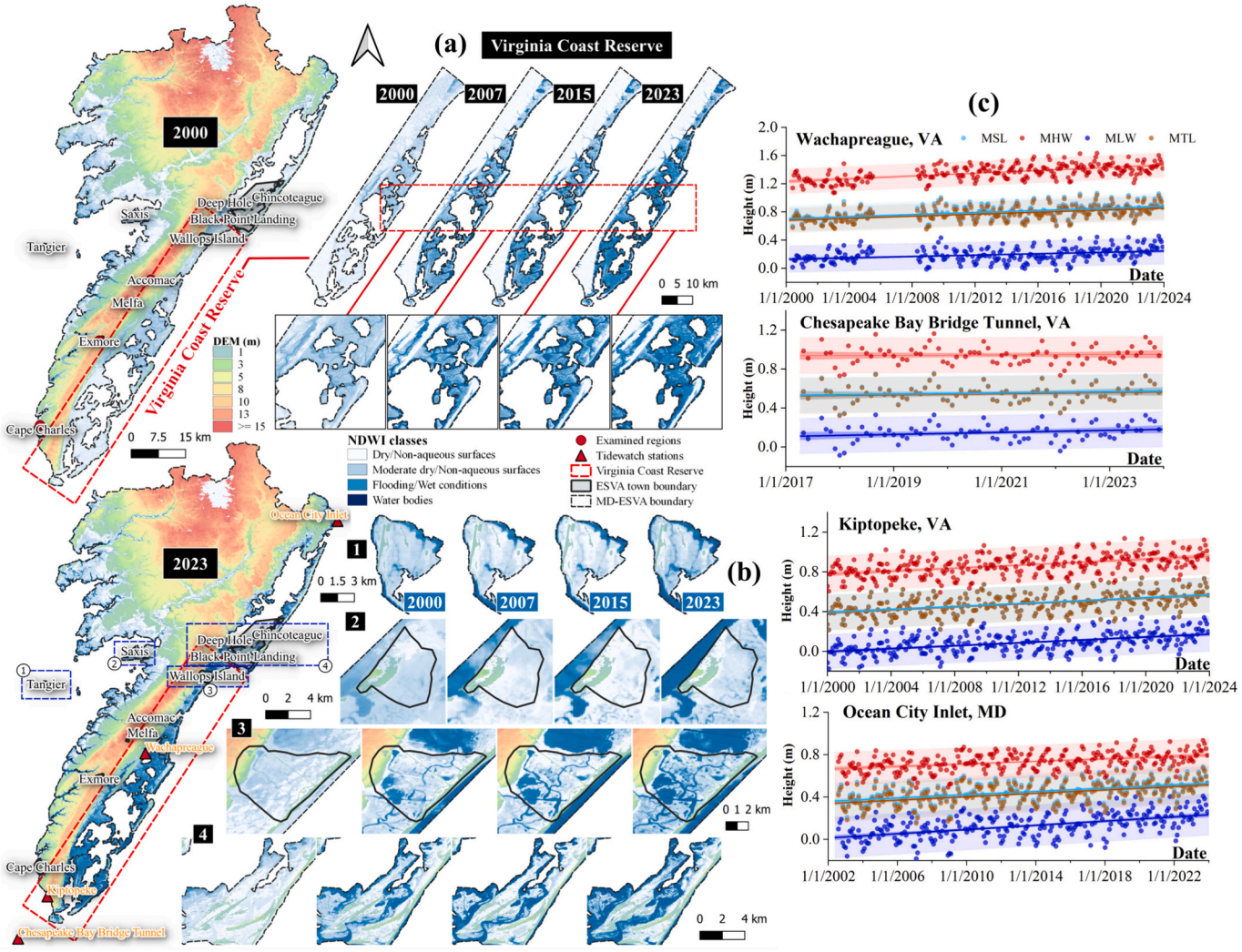

Fig. 9. Historical coastal seawater changes (2000–2023) for (a) VCR and (b) examining sites, including (1) Tangier, (2) Saxis, (3) Wallops Island, (4) Deep Hole, Chincoteague, and Black Point Landing. The historical mean sea level (MSL), mean high water (MHW), mean low water (MLW), and mean tide level (MTL) are shown in (c).

inundation and coastal-induced flooding due to SLR, further aggravating these issues, not only for groundwater but also for surface water, particularly ponds, which have recently been identified as emerging pollution sources in ESVA (Charlie, 2023). Additionally, while ESVA is known for its agricultural and poultry farming activities, the challenges posed by these industries are likely to be severely heightened by future inland and coastal flooding. A common issue identified is the exposure of residual manure to rain on poultry farms, allowing pollutants to enter the natural runoff through nearby streams (Tom, 2020) or percolate to deeper soil-water layers. Moreover, Russ (2020) indicated an increasing disappearance of family farms in ESVA as rising seawater gradually reduces soil productivity. This implies that severe impacts from SLR towards 2100, as presented in our work, could then transform these farmlands into significant sources of pesticides and poultry waste. Furthermore, farmers' practice of spreading untreated manure, rich in nitrogen and phosphorus, on the land exacerbates this problem. In normal conditions, the land can only absorb a limited amount of these chemicals (Kobell et al., 2015), which then highlights excess contamination in groundwater and land under this future context. In general, these challenges are likely to deteriorate living conditions in ESVA. Therefore, we propose the following recommendations for authorities and decision-makers:

- Implement regulations and establish documentation to monitor both current and unused accommodations, as well as farmland, to reduce pollution from household and agricultural disposals.
- Control the population in highly populated towns and regions to mitigate the impacts of regional flooding and extreme heat on human health.
- Construct additional levees and disaster protection barriers using environmentally friendly materials along the coast.

5. Conclusions

In this study, we performed an in-depth analysis to quantify the anticipated changes in future extremes along with demographics, LULC changes, and SLR over ESVA, Virginia. Our work features the IPCC AR6 report on the use of GCMs and SSPs, in which we highlight the importance of understanding the correlation between hydroclimatic extremes and societal components. Main findings are summarized, as follows:

(1) A notable increasing trend is found in meteorological conditions that lead to an increase in both the intensity and frequency of climate extremes over ESVA. Our findings indicate a transition from a dry (2024-2044) to a wetter condition (2045–2100), with

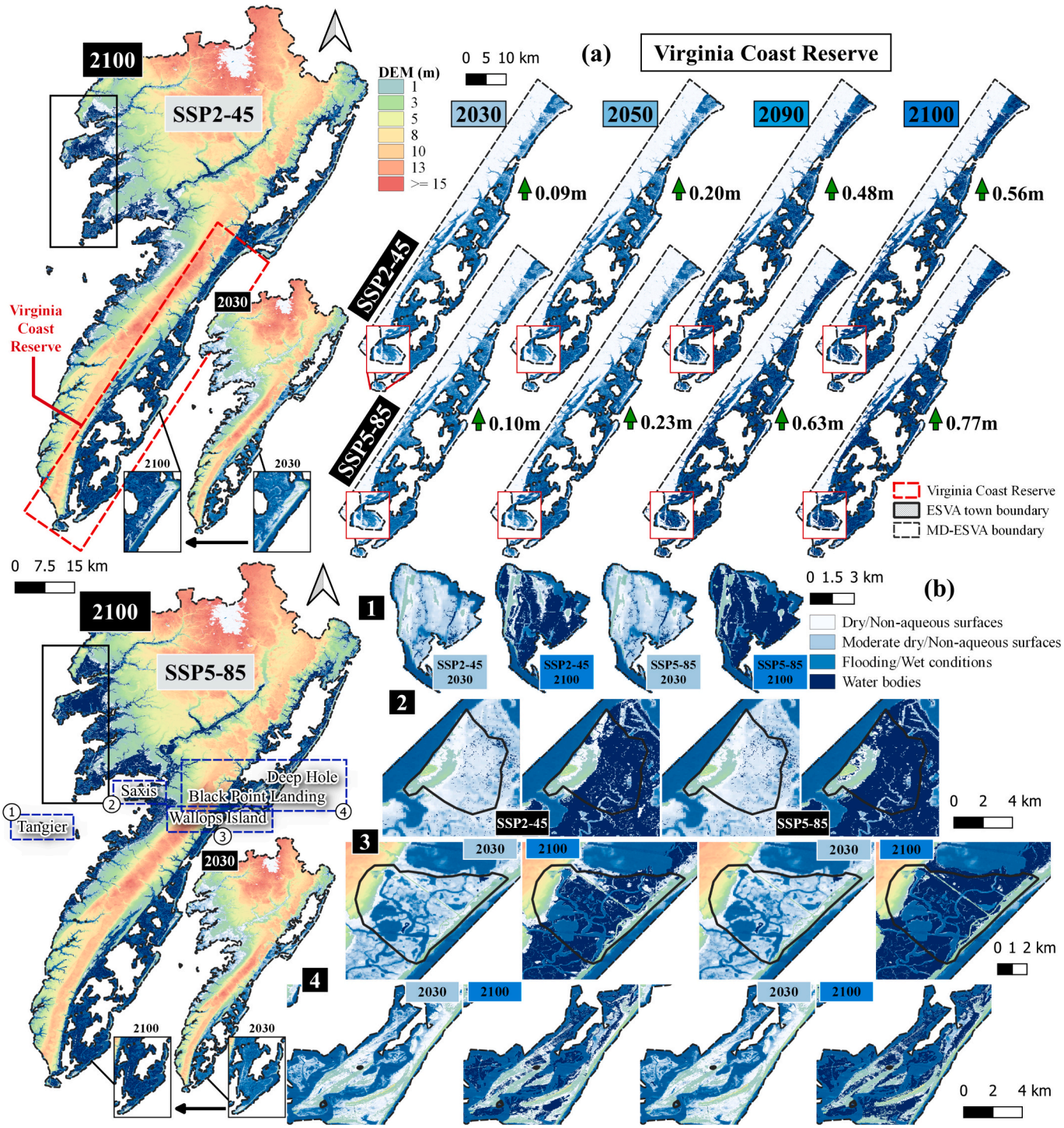

Fig. 10. Projected SLR over MD-ESVA and examined regions over ESVA (1) Tangier, (2) Saxis, (3) Wallops Island, (4) Deep Hole, Chincoteague, and Black Point Landing, and VCR under the SSP 2–45 and 5–85 scenarios between 2030 and 2100.

increases in flood peaks ranging from 3.41 % to 8.65 % during the mid future and up to 8.9 % in the far future.

(2) High-risk regions, identified using historical data of coastal hazards, demographics, and LULC, are projected to be more susceptible to future climate impacts. Under future extreme meteorological conditions, these regions could face severe impacts such as heat-related illnesses, and surface and groundwater pollution. Besides, these issues could be exacerbated by the increase in population and concrete-based infrastructure, especially in developed and economically oriented regions.

(3) Historical coastal risk caused by SLR was identified, while the current low-lying and coastal regions of the ESVA are projected to be more vulnerable to coastal- and SLR-induced flooding towards 2100, in which higher greenhouse gas emission scenario shows more profound impacts.

By incorporating human factors into our approach, we highlight the significant potential for ensuring the region's long-term resilience and safety against the challenges posed by climate change and human activities. Consequently, this work is a valuable resource for stakeholders

and regional authorities, assisting them in implementating sustainable strategies focused on disaster prevention and effective management of the region's water resources.

CRediT authorship contribution statement

Thanh-Nhan-Duc Tran: Writing – review & editing, Writing – original draft, Visualization, Validation, Software, Resources, Methodology, Investigation, Formal analysis, Data curation, Conceptualization. **Venkataraman Lakshmi:** Writing – review & editing, Supervision.

Declaration of competing interest

The authors declare that they have no known competing financial interests or personal relationships that could have appeared to influence the work reported in this paper.

Data availability

Data will be made available on request.

Acknowledgments

We acknowledge the support of Dr. Michele Claibourn, Dr. Elizabeth Mitchell, and Ms. Lauren Brideau from the University of Virginia (UVA) Equity Center and the UVA Department of Environmental Sciences in this work. We also want to express our special thanks to the authorities, stakeholders, and locals from the Eastern Shore of Virginia for their insightful and constructive comments during the 2024 ESVA Climate Equity Workshop in Melfa, Virginia. Last and foremost, we want to thank reviewers and the National Science Foundation (NSF; Grant No. 2053013, Coastlines and People) for their significant support in this study.

Appendix A. Supplementary data

Supplementary data to this article can be found online at https://doi.org/10.1016/j.scitotenv.2024.174289.

References

Adrian, L.-B., Nielsen, A., Castellanos-osorio, G., Trolle, D., Senent-aparicio, J., 2023. DSOLMap, a novel high-resolution global digital soil property map for the SWAT+ model: development and hydrolo- gical evaluation. Catena (Amst) 231. https://doi.org/10.1016/j.catena.2023.107339.

Ahmed, Z., Tran, T.N.D., Nguyen, Q.B., 2020. Applying semi distribution hydrological model SWAT to assess hydrological regime in Lai Giang catchment, Binh Dinh Province, Vietnam. In: Proceedings of the 2nd Conference on Sustainability in Civil Engineering (CSCE'20), Capital University of Science and Technology, Islamabad, Pakistan, 8.

Andrews, E., Kraus, J., West, A., 2019. Flooding and Sea Level Rise on the Eastern Shore.

A-NPDC, 2022. Accomack-Northampton Planning District Commission: Eastern Shore of Virginia Regional Housing Study. Eastern Shore of Virginia Housing Alliance; Accomack-Northampton Planning District Commission.

Arnold, J.G., Moriasi, D.N., Gassman, P.W., Abbaspour, K.C., White, M.J., Srinivasan, R., Santhi, C., Harmel, R.D., Van Griensven, A., Van Liew, M.W., Kannan, N., Jha, M.K., 2012. SWAT: model use, calibration, and validation. Trans. ASABE 55, 1491–1508. https://doi.org/10.13031/2013.42256.

Aryal, A., Tran, T.N.D., Kumar, B., Lakshmi, V., 2023. Evaluation of satellite-derived precipitation products for streamflow simulation of a mountainous Himalayan watershed: a study of Myagdi Khola in Kali Gandaki. Remote Sens. 15, 47–62. https://doi.org/10.3390/rs15194762.

Ashrafi, S., Kerachian, R., Pourmoghim, P., Behboudian, M., Motlaghzadeh, K., 2022. Evaluating and improving the sustainability of ecosystem services in river basins under climate change. Sci. Total Environ. 806 https://doi.org/10.1016/j.scitotenv.2021.150702.

Baills, A., Garcin, M., Bulteau, T., 2020. Assessment of selected climate change adaptation measures for coastal areas. Ocean Coast. Manag. 185 https://doi.org/10.1016/j.ocecoaman.2019.105059.

Bonsoms, J., Oliva, M., Alonso-González, E., Revuelto, J., López-Moreno, J.I., 2023. Impact of climate change on snowpack dynamics in coastal Central-Western Greenland. Sci. Total Environ. 169616 https://doi.org/10.1016/j.scitotenv.2023.169616.

Bounoua, L., Nigro, J., Zhang, P., Thome, K., Lachir, A., 2018. Mapping urbanization in the United States from 2001 to 2011. Appl. Geogr. 90, 123–133. https://doi.org/10.1016/j.apgeog.2017.12.002.

Brideau, L., Claibourn, M., Mitchell, E., Tran, T.-N.-D., Lakshmi, V., 2024. ESVA Climate Equity Workshop, Station 3: How Do Floods Affect People of the Eastern Shore Differently? Melfa, Virgnia.

C3S, 2024. Climate Indicators: Glaciers [WWW Document]. European Commission. URL climate.copernicus.eu/climate-indicators (accessed 5.8.24).

Charlie, P., 2023. Scientists Study Natural Processes Affecting Eastern Shore Aquifers [WWW Document]. Virginia Mercury. https://virginiamercury.com/2023/06/22/scientists-study-natural-processes-affecting-eastern-shore-aquifers/. (Accessed 26 February 2024).

Chen, B., Xie, M., Feng, Q., Li, Z., Chu, L., Liu, Q., 2021. Heat risk of residents in different types of communities from urban heat-exposed areas. Sci. Total Environ. 768 https://doi.org/10.1016/j.scitotenv.2021.145052.

Chen, C., Gan, R., Feng, D., Yang, F., Zuo, Q., 2022. Quantifying the contribution of SWAT modeling and CMIP6 inputting to streamflow prediction uncertainty under climate change. J. Clean. Prod. 364, 132675 https://doi.org/10.1016/j.jclepro.2022.132675.

Cheng, X., Chen, L., Sun, R., Kong, P., 2018. Land use changes and socio-economic development strongly deteriorate river ecosystem health in one of the largest basins in China. Sci. Total Environ. 616–617, 376–385. https://doi.org/10.1016/j.scitotenv.2017.10.316.

Chesapeake Bay Foundation, 2018. Virginia's Eastern Shore. Chesapeake Bay Foundation.

DEQ, 2024. Drought Watch Advisory Lifted for Much of Virginia [WWW Document]. CBS 19 News. URL. https://www.cbs19news.com/story/50355819/drought-watch-advisory-lifted-for-much-of-virginia (accessed 2.26.24).

Dile, Y., Srinivasan, R., George, C., 2019. QGIS Interface for SWAT+(QSWAT+), version 1.2. 2. Texas AM University.

Eyring, V., Bony, S., Meehl, G.A., Senior, C.A., Stevens, B., Stouffer, R.J., Taylor, K.E., Dynamique, D.M., Pierre, I., Laplace, S., Ipsl, L.M.D., 2016. Overview of the Coupled Model Intercomparison Project Phase 6 (CMIP6) experimental design and organization. Geosci. Model Dev. 9, 1937–1958. https://doi.org/10.5194/gmd-9-1937-2016.

Farinotti, D., Huss, M., Fürst, J.J., Landmann, J., Machguth, H., Maussion, F., Pandit, A., 2019. A consensus estimate for the ice thickness distribution of all glaciers on Earth. Nat. Geosci. 12, 168–173. https://doi.org/10.1038/s41561-019-0300-3.

FEMA, 2010. Flood Maps and Zones Explained [WWW Document]. FEMA. URL. https://www.fema.gov/blog/fema-flood-maps-and-zones-explained (accessed 2.26.24).

FEMA, 2020a. Flood Insurance Study (FIS) [WWW Document]. URL. https://www.fema.gov/glossary/flood-insurance-study-fis (accessed 2.26.24).

FEMA, 2020b. Flood Insurance Rate Map (FIRM) [WWW Document]. URL. https://www.fema.gov/glossary/flood-insurance-rate-map-firm (accessed 2.26.24).

FEMA, 2023a. Flood Insurance [WWW Document]. URL. https://www.fema.gov/flood-insurance (accessed 2.26.24).

FEMA, 2023b. Risk Mapping, Assessment and Planning (Risk MAP) [WWW Document]. URL. https://www.fema.gov/flood-maps/tools-resources/risk-map (accessed 2.26.24).

Gao, B.C., 1996. NDWI - a normalized difference water index for remote sensing of vegetation liquid water from space. Remote Sens. Environ. 58, 257–266. https://doi.org/10.1016/S0034-4257(96)00067-3.

Gelaro, R., McCarty, W., Suárez, M.J., Todling, R., Molod, A., Takacs, L., Randles, C.A., Darmenov, A., Bosilovich, M.G., Reichle, R., Wargan, K., Coy, L., Cullather, R., Draper, C., Akella, S., Buchard, V., Conaty, A., da Silva, A.M., Gu, W., Kim, G.K., Koster, R., Lucchesi, R., Merkova, D., Nielsen, J.E., Partyka, G., Pawson, S., Putman, W., Rienecker, M., Schubert, S.D., Sienkiewicz, M., Zhao, B., 2017. The modern-era retrospective analysis for research and applications, version 2 (MERRA-2). J. Clim. 30, 5419–5454. https://doi.org/10.1175/JCLI-D-16-0758.1.

Gorelick, N., Hancher, M., Dixon, M., Ilyushchenko, S., Thau, D., Moore, R., 2017. Google earth engine: planetary-scale geospatial analysis for everyone. Remote Sens. Environ. 202, 18–27. https://doi.org/10.1016/j.rse.2017.06.031.

Gupta, H.V., Kling, H., Yilmaz, K.K., Martinez, G.F., 2009. Decomposition of the mean squared error and NSE performance criteria: implications for improving hydrological modelling. J Hydrol (Amst) 377, 80–91. https://doi.org/10.1016/j.jhydrol.2009.08.003.

Hausfather, Z., 2019. CMIP6: the next generation of climate models explained [WWW document]. In: Carbon Brief: Climate Modeling. URL. https://www.carbonbrief.org/cmip6-the-next-generation-of-climate-models-explained/ (accessed 2.26.24).

Hoehne, C.G., Hondula, D.M., Chester, M.V., Eisenman, D.P., Middel, A., Fraser, A.M., Watkins, L., Gerster, K., 2018. Heat exposure during outdoor activities in the US varies significantly by city, demography, and activity. Health Place 54, 1–10. https://doi.org/10.1016/j.healthplace.2018.08.014.

Hou, A.Y., Kakar, R.K., Neeck, S., Azarbarzin, A.A., Kummerow, C.D., Kojima, M., Oki, R., Nakamura, K., Iguchi, T., 2014. The global precipitation measurement mission. Bull. Am. Meteorol. Soc. 95, 701–722. https://doi.org/10.1175/BAMS-D-13-00164.1.

Hugonnet, R., McNabb, R., Berthier, E., Menounos, B., Nuth, C., Girod, L., Farinotti, D., Huss, M., Dussaillant, I., Brun, F., Kääb, A., 2021. Accelerated global glacier mass loss in the early twenty-first century. Nature 592, 726–731. https://doi.org/10.1038/s41586-021-03436-z.

IPCC, 2021. Climate Change 2021: The Physical Science Basis. Contribution of Working Group I to the Sixth Assessment Report of the Intergovernmental Panel on Climate Change.

IPCC, 2023. Ocean, cryosphere and sea level change. In: Climate Change 2021 – The Physical Science Basis. Cambridge University Press, pp. 1211–1362. https://doi.org/10.1017/9781009157896.011.
IPPC, 2021. Chapter Outline of the Working Group III Contribution to the IPCC Six Assessment Report (AR6).
Kjellstrom, T., Holmer, I., Lemke, B., 2009. Workplace heat stress, health and productivity-an increasing challenge for low and middle-income countries during climate change. Glob. Health Action 2. https://doi.org/10.3402/gha.v2i0.2047.
Kobell, R., Horton, T., Simpson, T., Summers, R.M., 2015. The Chesapeake Bay and Agricultural Pollution: The Problem, Possible Solutions, and the Need for Verification.
Lazo, J.K., Bostrom, A., Morss, R.E., Demuth, J.L., Lazrus, H., 2015. Factors affecting hurricane evacuation intentions. Risk Anal. 35, 1837–1857. https://doi.org/10.1111/risa.12407.
Lehner, B., Grill, G., 2013. Global river hydrography and network routing: baseline data and new approaches to study the world's large river systems. Hydrol. Process. 27, 2171–2186. https://doi.org/10.1002/hyp.9740.
Maurer, E.P., Hidalgo, H.G., 2008. Utility of daily vs. monthly large-scale climate data: an intercomparison of two statistical downscaling methods. Hydrol. Earth Syst. Sci. 12, 551–563. https://doi.org/10.5194/hess-12-551-2008.
Maurer, E.P., Kayser, G., Doyle, L., Wood, A.W., 2018. Adjusting flood peak frequency changes to account for climate change impacts in the Western United States. J. Water Resour. Plan. Manag. 144 https://doi.org/10.1061/(asce)wr.1943-5452.0000903.
McFeeters, S.K., 1996. The use of the normalized difference water index (NDWI) in the delineation of open water features. Int. J. Remote Sens. 17, 1425–1432. https://doi.org/10.1080/01431169608948714.
Merz, B., Basso, S., Fischer, S., Lun, D., Blöschl, G., Merz, R., Guse, B., Viglione, A., Vorogushyn, S., Macdonald, E., Wietzke, L., Schumann, A., 2022. Understanding heavy tails of flood peak distributions. Water Resour. Res. https://doi.org/10.1029/2021WR030506.
Meyer, L., 2015. IPCC Fifth Assessment Report Synthesis Report Key Messages.
Moriasi, D.N., Gitau, M.W., Pai, N., Daggupati, P., 2015. Hydrologic and water quality models: performance measures and evaluation criteria. Trans. ASABE 58, 1763–1785. https://doi.org/10.13031/trans.58.10715.
NASA, 2024. America's sinking East Coast [WWW Document]. NASA Earth Observatory. URL. https://earthobservatory.nasa.gov/images/152452/americas-sinking-east-coast (accessed 2.26.24).
Nash, J.E., Sutcliffe, J.V., 1970. River flow forecasting through conceptual models part I—a discussion of principles. J Hydrol (Amst) 10, 282–290. https://doi.org/10.1016/0022-1694(70)90255-6.
Neill, B.C.O., Tebaldi, C., Vuuren, D. Van, Eyring, V., Hurtt, G., Knutti, R., Kriegler, E., Lamarque, J., 2016. The Scenario Model Intercomparison Project (ScenarioMIP) for CMIP6. Geosci. Model Dev. 1–35. https://doi.org/10.5194/gmd-2016-84.
Nghia, B.P.Q., Pal, I., Pramanik, M., Dasgupta, R., 2022a. The impact of climate change on drought and its adaptation strategies: findings from general circulation models and households in Tien Giang Province, Vietnam. Clim. Chang. 175 https://doi.org/10.1007/s10584-022-03473-1.
Nghia, B.P.Q., Pal, I., Chollacoop, N., Mukhopadhyay, A., 2022b. Applying Google earth engine for flood mapping and monitoring in the downstream provinces of Mekong river. Progress in Disaster Science 14. https://doi.org/10.1016/j.pdisas.2022.100235.
Nguyen, T.V., Dietrich, J., Dang, T.D., Tran, D.A., Van Doan, B., Sarrazin, F.J., Abbaspour, K., Srinivasan, R., 2022. An interactive graphical interface tool for parameter calibration, sensitivity analysis, uncertainty analysis, and visualization for the Soil and Water Assessment Tool. Environ. Model. Softw. 156 https://doi.org/10.1016/j.envsoft.2022.105497.
Nguyen, B.Q., Kantoush, S., Binh, D. Van, Saber, M., Vo, D.N., Sumi, T., 2022a. Understanding the anthropogenic development impacts on long-term flow regimes in a tropical river basin, Central Vietnam. Hydrol. Sci. J. https://doi.org/10.1080/02626667.2022b.2153298.
Nguyen, B.Q., Tran, T.N.D., Grodzka-Łukaszewska, M., Sinicyn, G., Lakshmi, V., 2022b. Assessment of urbanization-induced land-use change and its impact on temperature, evaporation, and humidity in Central Vietnam. Water (Switzerland) 14. https://doi.org/10.3390/w14213367.
Nguyen, B.Q., Kantoush, S., Binh, D. Van, Saber, M., Vo, D.N., Sumi, T., 2023a. Quantifying the impacts of hydraulic infrastructure on tropical streamflows. Hydrol. Process. 37 https://doi.org/10.1002/hyp.14834.
Nguyen, B.Q., Kantoush, S.A., Tran, T.-N.-D., Binh, D. Van, Vo, N.D., Saber, M., Sumi, T., 2023b. Response of Hydrological to Anthropogenic Activities in a Tropical Basin, pp. 269–278. https://doi.org/10.3850/978-90-833476-1-5_iahr40wc-p1339-cd.
Nguyen, B.Q., Van Binh, D., Kantoush, S.A., Sumi, T., 2024. Response of streamflow and sediment variability to cascade dam development and climate change in the Sai Gon Dong Nai River basin. Clim. Dyn. https://doi.org/10.1007/s00382-024-07319-7.
NOAA, 2001. Sea, Lake, and Overland Surges from Hurricanes (SLOSH) [WWW Document]. URL. https://www.nhc.noaa.gov/surge/slosh.php (accessed 2.26.24).
NOAA, 2010. Tides and Current [WWW Document]. URL. https://tidesandcurrents.noaa.gov/map/index.html (accessed 5.8.24).
NOAA, 2020. July 2020 Drought Report.
NOAA, 2024a. Coastal Flood Hazard Composite Layer for the Coastal Flood Exposure Mapper [WWW Document]. URL. https://coast.noaa.gov/floodexposure/#-10575352,4439107,5z (accessed 2.26.24).
NOAA, 2024b. 2023 Was the World's Warmest Year on Record, by Far [WWW Document]. URL. https://www.noaa.gov/news/2023-was-worlds-warmest-year-on-record-by-far.
Nowroozi, A.A., Horrocks, S.B., Henderson, P., 1999. Saltwater intrusion into the freshwater aquifer in the eastern shore of Virginia: a reconnaissance electrical resistivity survey. J. Appl. Geophys. 42 https://doi.org/10.1016/S0926-9851(99)00004-X.
O'Donoghue, S., Lehmann, M., Major, D., Major-Ex, G., Sutherland, C., Motau, A., Haddaden, N., Kibria, A.S., Costanza, R., Groves, C., Behie, A., Johnson, K., 2021. Adaptation to climate change in small coastal cities: the influence of development status on adaptation response. Ocean Coast. Manag. 211 https://doi.org/10.1016/j.ocecoaman.2021.105788.
Ohenhen, L.O., Shirzaei, M., Ojha, C., Kirwan, M.L., 2023. Hidden vulnerability of US Atlantic coast to sea-level rise due to vertical land motion. Nat. Commun. 14 https://doi.org/10.1038/s41467-023-37853-7.
Oleson, K.W., Monaghan, A., Wilhelmi, O., Barlage, M., Brunsell, N., Feddema, J., Hu, L., Steinhoff, D.F., 2015. Interactions between urbanization, heat stress, and climate change. Clim. Chang. 129, 525–541. https://doi.org/10.1007/s10584-013-0936-8.
Park, T., Hashimoto, H., Wang, W., Thrasher, B., Michaelis, A.R., Lee, T., Brosnan, I.G., Nemani, R.R., 2023. What does global land climate look like at 2°C warming? Earths Future 11, 1–16. https://doi.org/10.1029/2022EF003330.
Peng, S., Wang, C., Li, Z., Mihara, K., Kuramochi, K., Toma, Y., Hatano, R., 2023. Climate change multi-model projections in CMIP6 scenarios in Central Hokkaido, Japan. Sci. Rep. 13, 1–18. https://doi.org/10.1038/s41598-022-27357-7.
Pignotti, G., Rathjens, H., Cibin, R., Chaubey, I., Crawford, M., 2017. Comparative analysis of HRU and grid-based SWAT models. Water (Switzerland) 9, 272. https://doi.org/10.3390/w9040272.
Raftery, A.E., Zimmer, A., Frierson, D.M.W., Startz, R., Liu, P., 2017. Less than 2 °c warming by 2100 unlikely. Nat. Clim. Chang. 7, 637–641. https://doi.org/10.1038/nclimate3352.
Ralph, T.W., George Carrington, M., 1952. Virginia's Eastern Shore: A History of Northampton and Accomack Counties. Virginia Historical Society.
Rebecca, L., 2022. Climate Change: Global Sea Level [WWW Document]. NOAA Climate GOV. URL. https://www.climate.gov/news-features/understanding-climate/climate-change-global-sea-level (accessed 2.26.24).
Ren, J., Wang, W., Wei, J., Li, H., Li, X., Liu, G., Chen, Y., Ye, S., 2023. Evolution and prediction of drought-flood abrupt alternation events in Huang-Huai-Hai River Basin, China. Sci. Total Environ. 869 https://doi.org/10.1016/j.scitotenv.2023.161707.
Rosenzweig, C., Neofotis, P., 2013. Detection and attribution of anthropogenic climate change impacts. Wiley Interdiscip. Rev. Clim. Chang. 4, 121–150. https://doi.org/10.1002/wcc.209.
Russ, B., 2020. A Sea Change For The Eastern Shore [WWW Document]. University of Virginia. URL. https://give.as.virginia.edu/news/story/sea-change-eastern-shore.
Saadi, Z., Alias, N.E., Yusop, Z., Iqbal, Z., Houmsi, M.R., Houmsi, L.N., Ramli, M.W.A., Muhammad, M.K.I., 2024. Application of relative importance metrics for CMIP6 models selection in projecting basin-scale rainfall over Johor River basin, Malaysia. Sci. Total Environ. 912 https://doi.org/10.1016/j.scitotenv.2023.169187.
Saeedi, M., Nabaei, S., Kim, H., Tavakol, A., Lakshmi, V., 2023. Performance assessment of SM2RAIN-NWF using ASCAT soil moisture via supervised land cover-soil-climate classification. Remote Sens. Environ. 285 https://doi.org/10.1016/j.rse.2022.113393.
Saleem, F., Zeng, X., Hina, S., Omer, A., 2021. Regional changes in extreme temperature records over Pakistan and their relation to Pacific variability. Atmos. Res. 250 https://doi.org/10.1016/j.atmosres.2020.105407.
Sanford, W.E., Pope, J.P., 2007. A simulation of groundwater discharge and nitrate delivery to Chesapeake Bay from the lowermost Delmarva Peninsula, USA. In: IAHS-AISH Publication, pp. 326–333.
Sanford, W.E., Pope, J.P., 2010. Current challenges using models to forecast seawater intrusion: lessons from the Eastern Shore of Virginia, USA. Hydrogeol. J. 18, 73–93. https://doi.org/10.1007/s10040-009-0513-4.
Shafeeque, M., Hafeez, M., Sarwar, A., Arshad, A., Khurshid, T., 2023. Quantifying future water saving potential under climate change and groundwater recharge scenarios in Lower Chenab Canal. Indus River Basin. Theor Appl Climatol. https://doi.org/10.1007/s00704-023-04621-y.
Shrestha, S., Bhatta, B., Shrestha, M., Shrestha, P.K., 2018. Integrated assessment of the climate and landuse change impact on hydrology and water quality in the Songkhram River Basin, Thailand. Sci. Total Environ. 643, 1610–1622. https://doi.org/10.1016/j.scitotenv.2018.06.306.
Skeo, S., 2015. Indoor Plumbing Needs on the Eastern Shore of Virginia Prepared for the Accomack-Northampton Planning District Commission.
Smith, A., 2024. 2023: A historic year of U.S. billion-dollar weather and climate disasters. NOAA Climate.
Svoboda, M., Lecomte, D., Hayes, M., Heim, R., Gleason, K., Angel, J., Rippey, B., Tinker, R., Palecki, M., Stooksbury, D., Miskus, D., Stephens, S., 2002. The drought monitor. Bull. Am. Meteorol. Soc. 1181–1190. https://doi.org/10.1175/1520-0477-83.8.1181.
Tarboton, D.G., 2011. A Tutorial for Using TauDEM to Delineate a Single Watershed.
Tebaldi, C., Debeire, K., Eyring, V., Fischer, E., Fyfe, J., Friedlingstein, P., Knutti, R., Lowe, J., O'Neill, B., Sanderson, B., Van Vuuren, D., Riahi, K., Meinshausen, M., Nicholls, Z., Tokarska, K., Hurtt, G., Kriegler, E., Meehl, G., Moss, R., Bauer, S., Boucher, O., Brovkin, V., Yhb, Y., Dix, M., Gualdi, S., Guo, H., John, J., Kharin, S., Kim, Y.H., Koshiro, T., Ma, L., Olivié, D., Panickal, S., Qiao, F., Rong, X., Rosenbloom, N., Schupfner, M., Séférian, R., Sellar, A., Semmler, T., Shi, X., Song, Z., Steger, C., Stouffer, R., Swart, N., Tachiiri, K., Tang, Q., Tatebe, H., Voldoire, A., Volodin, E., Wyser, K., Xin, X., Yang, S., Yu, Y., Ziehn, T., 2021. Climate model projections from the Scenario Model Intercomparison Project (ScenarioMIP) of CMIP6. Earth Syst. Dynam. 12, 253–293. https://doi.org/10.5194/esd-12-253-2021.
Thrasher, B., Wang, W., Michaelis, A., Melton, F., Lee, T., Nemani, R., 2022. NASA global daily down-scaled projections, CMIP6. Sci Data 9, 1–6. https://doi.org/10.1038/s41597-022-01393-4.

Toimil, A., Losada, I.J., Nicholls, R.J., Dalrymple, R.A., Stive, M.J.F., 2020. Addressing the challenges of climate change risks and adaptation in coastal areas: a review. Coast. Eng. https://doi.org/10.1016/j.coastaleng.2019.103611.
Tom, P., 2020. Poultry and Manure Production on Virginia's Eastern Shore Rapid Growth and Poor Environmental Compliance Threaten Waterways in Accomack County.
Tran, T.-N.-D., Do, S.K., Nguyen, B.Q., Tran, V.N., Grodzka-Lukaszewska, M., Sinicyn, G., Lakshmi, V., 2024a. Investigating the future flood and drought shifts in the transboundary Srepok River basin using CMIP6 projections. IEEE J Sel Top Appl Earth Obs Remote Sens 17, 7516–7529. https://doi.org/10.1109/JSTARS.2024.3380514.
Tran, T.-N.-D., Lakshmi, V., 2022. The land use changes impacts on socio-economic drivers and simulation of surface and groundwater in the Eastern Shore of Virginia, the United States. AGU Fall Meeting Abstracts 2022, H42D–1270.
Tran, T.-N.-D., Nguyen, Q.B., Zeeshan, A., 2021a. Application of plaxis for calculating the construction stability and soft embankment in protecting Ha Thanh. In: 2nd Conference on Sustainability in Civil Engineering (CSCE) 2020, pp. 202–210.
Tran, T.N.D., Ahmed, Z., Vo, N.D., 2021b. Application of hydrodynamic modelling to assess the efficiency of hurricane protection measure at Xom Ro Dike, Phu Yen Province, Vietnam. In: 2nd Conference on Sustainability in Civil Engineering (CSCE'20). Department of Civil Engineering Capital University of Science and Technology, Islamabad Pakistan.
Tran, T.N.D., Nguyen, Q.B., Vo, N.D., Marshall, R., Gourbesville, P., 2022a. Assessment of terrain scenario impacts on hydrological simulation with SWAT model. In: Application to Lai Giang Catchment, Vietnam. Springer Water. Springer Nature, pp. 1205–1222. https://doi.org/10.1007/978-981-19-1600-7_77.
Tran, T.N.D., Nguyen, Q.B., Tam, D., Le, L., Nguyen, T.D., Vo, N.D., Gourbesville, P., 2022b. Evaluate the influence of Groynes system on the hydraulic regime in the Ha Thanh River, Binh Dinh Province, Vietnam. In: Advances in Hydroinformatics, pp. 241–254. https://doi.org/10.1007/978-981-19-1600-7_15.
Tran, T.N.D., Nguyen, Q.B., Nguyen, T.T., Vo, N.D., Nguyen, C.P., Gourbesville, P., 2022c. Operational methodology for the assessment of typhoon waves characteristics. In: Application to Ninh Thuan Province, Vietnam. Springer Water. Springer Nature, pp. 887–902. https://doi.org/10.1007/978-981-19-1600-7_55.
Tran, T.-N.-D., Le, M.-H., Zhang, R., Nguyen, B.Q., Bolten, J.D., Lakshmi, V., 2023a. Robustness of gridded precipitation products for Vietnam basins using the comprehensive assessment framework of rainfall. Atmos. Res. 293, 106923 https://doi.org/10.1016/j.atmosres.2023.106923.
Tran, T.-N.-D., Nguyen, B.Q., Grodzka-Łukaszewska, M., Sinicyn, G., Lakshmi, V., 2023b. The role of reservoirs under the impacts of climate change on the Srepok River basin, Central Highlands of Vietnam. Front. Environ. Sci. 11 https://doi.org/10.3389/fenvs.2023.1304845.
Tran, T.N.D., Nguyen, B.Q., Vo, N.D., Le, M.H., Nguyen, Q.D., Lakshmi, V., Bolten, J.D., 2023c. Quantification of global Digital Elevation Model (DEM) – a case study of the newly released NASADEM for a river basin in Central Vietnam. J Hydrol Reg Stud 45. https://doi.org/10.1016/j.ejrh.2022.101282.
Tran, T.N.D., Nguyen, B.Q., Zhang, R., Aryal, A., Grodzka-Łukaszewska, M., Sinicyn, G., Lakshmi, V., 2023d. Quantification of gridded precipitation products for the streamflow simulation on the Mekong River Basin using rainfall assessment framework: a case study for the Srepok River subbasin, Central Highland Vietnam. Remote Sens. 15 https://doi.org/10.3390/rs15041030.
Tran, T.-N.-D., Tapas, M.R., Do, S.K., Etheridge, R., Lakshmi, V., 2024b. Investigating the impacts of climate change on hydroclimatic extremes in the Tar-Pamlico River basin, North Carolina. J. Environ. Manage. 363 https://doi.org/10.1016/j.jenvman.2024.121375.
U.S Census Bureau, 2023. American Community Survey 5-Year Data (2009–2021).
U.S. Census Bureau, 2007. LODESTechDoc8.0.
U.S. Census Bureau, 2010. LED New Data from the States and the U.S. Census Bureau: Local Employment Dynamics.
U.S. Census Bureau, 2022. Nation's Urban and Rural Populations Shift Following 2020 Census [WWW Document]. https://www.census.gov/newsroom/press-releases/2022/urban-rural-populations.html.
U.S. Fish & Wildlife Service, 2018. Eastern Shore of Virginia National Wildlife Refuge. U.S. Fish & Wildlife Service.
UN Population Division, 2018. World Urbanization Prospects: The 2018 Revision.
USGS, 2020. Land change monitoring, assessment, and projection. U.S. Geological Survey Fact Sheet 2020, 1–4. https://doi.org/10.3133/fs20203024.
Villarini, G., Smith, J.A., 2010. Flood peak distributions for the eastern United States. Water Resour. Res. 46 https://doi.org/10.1029/2009WR008395.
Wan, X., Wang, W., Liu, J., Tong, T., 2014. Estimating the sample mean and standard deviation from the sample size, median, range and/or interquartile range. BMC Med. Res. Methodol. 14, 135. https://doi.org/10.1186/1471-2288-14-135.
Wang, T., Tu, X., Singh, V.P., Chen, X., Lin, K., 2021. Global data assessment and analysis of drought characteristics based on CMIP6. J Hydrol (Amst) 596, 126091. https://doi.org/10.1016/j.jhydrol.2021.126091.
Wayne, C., 2022. Short-term Rentals, Long-term Headaches [WWW Document]. URL. http://www.capecharlesmirror.com/short-term-rentals-long-term-headaches/ (accessed 2.26.24).
Webb, N.P., Marshall, N.A., Stringer, L.C., Reed, M.S., Chappell, A., Herrick, J.E., 2017. Land degra- dation and climate change: building climate resilience in agriculture. Front. Ecol. Environ. 15, 450–459. https://doi.org/10.1002/fee.1530.
Wood, A.W., Maurer, E.P., Kumar, A., Lettenmaier, D.P., 2002. Long-range experimental hydrologic fore- casting for the eastern United States. J. Geophys. Res. Atmos. 107 (ACL 6-1-ACL), 6–15. https://doi.org/10.1029/2001JD000659.
Wood, A.W., Leung, L.R., Sridhar, V., Lettenmaier, D.P., 2004. Hydrologic implications of dynamical and statistical approaches to downscaling climate model outputs. Clim. Chang. 62, 189–216. https://doi.org/10.1023/B:CLIM.0000013685.99609.9e.
Xu, X., Yun, X., Tang, Q., Cui, H., Wang, J., Zhang, L., Chen, D., 2023. Projected seasonal changes in future rainfall erosivity over the Lancang-Mekong River basin under the CMIP6 scenarios. J Hydrol (Amst) 620, 129444. https://doi.org/10.1016/j.jhydrol.2023.129444.
Yamazaki, D., Ikeshima, D., Sosa, J., Bates, P.D., Allen, G.H., Pavelsky, T.M., 2019. MERIT hydro: a high-resolution global hydrography map based on latest topography dataset. Water Resour. Res. 55, 5053–5073. https://doi.org/10.1029/2019WR024873.
Yin, Y., Wu, Y., Bartell, S.M., Cosgriff, R., 2009. Patterns of forest succession and impacts of flood in the Upper Mississippi River floodplain ecosystem. Ecol. Complex. 6, 463–472. https://doi.org/10.1016/j.ecocom.2009.08.004.
Yin, C., Yuan, M., Lu, Y., Huang, Y., Liu, Y., 2018. Effects of urban form on the urban heat island effect based on spatial regression model. Sci. Total Environ. 634, 696–704. https://doi.org/10.1016/j.scitotenv.2018.03.350.
Zambello, E., 2019. LTER Road Trip: A Changing Landscape along Virginia's Eastern Shore.
Zhang, H., Qi, Z. Fang, Ye, X. Yue, Cai, Y. Bin, Ma, W. Chun, Chen, M. Nan, 2013. Analysis of land use/land cover change, population shift, and their effects on spatiotemporal patterns of urban heat islands in metropolitan Shanghai, China. Appl. Geogr. 44, 121–133. https://doi.org/10.1016/j.apgeog.2013.07.021.
Zhong, R., Zhao, T., Chen, X., Jin, H., 2022. Monitoring drought in ungauged areas using satellite altimetry: the standardized river stage index. J Hydrol (Amst) 612, 128308. https://doi.org/10.1016/j.jhydrol.2022.128308.
Zhou, X., Chen, H., 2018. Impact of urbanization-related land use land cover changes and urban morphology changes on the urban heat island phenomenon. Sci. Total Environ. 635, 1467–1476. https://doi.org/10.1016/j.scitotenv.2018.04.091.